Structures related to the emplacement of shallow-level intrusions

David Westerman, Sergio Rocchi, Christoph Breitkreuz, Carl Stevenson, Penelope Wilson

1. Norwich University, VT, USA
2. Università di Pisa, Italy
3. TU Bergakademie, Freiberg, Germany
4. University of Birmigham, UK
5. Kingston University, London, UK

Abstract

A systematic view of the vast nomenclature used to describe the structures of shallow level intrusions is presented here. Structures are organised in four main groups, according to logical breaks in the timing of magma emplacement, independent of the scales of features: (1) Intrusion-related structures, formed as the magma is making space and then develops into its intrusion shape; (2) Magmatic flow-related structures, developed as magma moves with suspended crystals that are free to rotate; (3) Solid-state, flow-related structures that formed in portions of the intrusions affected by continuing flow of nearby magma, therefore considered to have a syn-magmatic, non-tectonic origin; (4) Thermal and fragmental structures, related to creation of space and impact on host materials. This scheme appears as a rational organisation, helpful in describing and interpreting the large variety of structures observed in shallow-level intrusions.

Keywords: Magma intrusion, Magma flow, Syn-magmatic deformation, Fragmentation, Geo-logic.

1. Introduction

This overview of the fabrics and structures characterizing shallow-level intrusions is focused on tabular intrusions recognized as dykes, sills and laccoliths, and related types of bodies. At the grossest scale, shallow-level intrusive bodies are classified based on their aspect ratio and relationship to pre-existing structures in their host, and on their coherent versus clastic texture. The simplest subdivision is generally to separate dykes, with their subparallel contacts cross cutting the host fabric, from sills (*s.l.*).

The latter group is further subdivided into sills (*s.s.*), laccoliths, and a host of more esoteric forms (Rocchi and Breitkreuz this volume). Sills are, for the most part, defined as tabular igneous intrusions that are concordant with planar structures in the surrounding host rocks (bedding, unconformities, or cleavage) and display large length:thickness ratios. Laccoliths and lopoliths are also concordant intrusions with a convex-upwards upper contact or a planar to concave-downwards lower contact, respectively. Laccoliths are distinguished from sills by the non-linear, inelastic, large-scale deflection of roof host rocks that accompanies their emplacement, and by their generally smaller length:thickness ratios (Corry 1988).

Because bodies such as dykes, sills and laccoliths develop by magma propagating along a planar surface, either by brittle or non-brittle failure, it is useful to acknowledge the time frame within which we are concerned. This chapter focuses on the interval between the arrival of the initial magma at its propagating fracture (a time before the igneous body was there at all) and the cessation of magmatic activity with development of younger fractures due to cooling (a time after it was there completely).

This broad scope reflects the transitional role that SLI play as an interface between the hidden kingdom of Pluto below and the fiery realm of Vulcan above. Although nearly all of the features discussed here have been previously recognized and described, including in some of the earliest writings on geology, our organization and coverage of this material can provide a framework to visualize the formation of SLI through time and space.

For the most part, SLI share the characteristic of having distinctive chilled margins, a population of phenocrysts, and generally aphanitic textures in the matrix. The simplest interpretation is that generally euhedral phenocrysts formed prior to arrival at the final emplacement level (Mock et al. 2003), and that solidification of the melt phase was rapid. Exceptions include thick mafic sills that are characterized by phaneritic textures, often with evidence of layering attributed to *in-situ* gravity settling (e.g.: 350-450 m-thick Basement Sill, Antarctica) (Bédard et al. 2007) and, more rarely, moderately thick (ca. 50 m) rhyolitic sills (Orth and McPhie 2003).

The scales of these features range from structures consisting of sets of intrusive bodies, to shapes and sizes of individual bodies, to scales related to maps, outcrops, hand specimens, thin sections and smaller. Also included are invisible properties such as anisotropy of magnetic susceptibility and chemical zonation.

The value of understanding the physical characteristics of these shallow intrusions lies in large part with the information they can provide about their modes of formation. Often of greatest interest is the use of these characteristics to unravel directions and styles of magma flow so as to understand the growth and development of these bodies.

Major works that bring the understanding of dykes to the forefront include papers collected in proceedings from the International Dyke Conference starting as far back as 1985 (Halls and Fahrig 1987). Papers of this volume, along with volumes resulting from previous LASI conferences since the first in 2002, provide a useful collection of modern work detailing the physical geology of laccoliths, dykes and sills (Breitkreuz and Petford 2004; Rocchi et al. 2010; Thomson and Petford 2008).

Principally, formation of all fabrics and structures featured here depends on fundamental physical parameters of the emplacing magma, such as temperature, driving pressure, viscosity, volume, ascent/emplacement rate and emplacement level, as well as yield strength and porosity of the host. Many of these parameters have been explored in other chapters of this volume.

Understanding of structures in sub-horizontal tabular intrusions starts with the generalized characteristics that have been addressed by examining expansive databases of sills and laccoliths as reported in the literature. The database of the first encyclopedic work (Corry 1988) recorded 900 laccoliths globally, 600 of which were from North America. The author extrapolated this number to infer that there were actually 5,000 to 10,000 laccoliths globally. This database has been expanded and the diameter and thickness values have been examined, discovering the power law relation between those values (Cruden and McCaffrey 2001; McCaffrey and Petford 1997). Subsequently, an S-shaped power law matching well with plutons of all scales has been proposed (Cruden and McCaffrey 2002), and further augmented and discussed by Cruden et al. this volume. The resulting models show consistent geometric relationships of these parameters.

The multi-layered laccoliths preserved on Elba Island have provided a number of examples that support published models (Cruden and McCaffrey 2002; Cruden and McCaffrey 2001), but also yield further understanding about the emplacement and inflation processes within such complexes (Rocchi et al. 2002) and the relationships of their geometries to those of assembled plutons (Rocchi et al. 2010).

The range of features associated with formation of tabular SLI is very broad. During emplacement and solidification, fabrics and structures develop in different locations within the bodies (interior vs. interface), from different driving forces (magmatic flow, solid-state flow, static gravity and thermal), and at various scales (from whole intrusion scale to microscale).

SLI are characterized first by generally having large aspect ratios with overall tabular forms, and second by emplacement into the coolest portion of the crust. These conditions lead to the relatively short “lifetimes” of these bodies between onset of emplacement and complete solidification. Compared to more deep-seated plutons, SLI end up dominated by fabrics and structures directly associated with emplacement since their typical quick crystallization limit the time available to fractionate and develop

features associated with *in-situ* crystallization. Thus, well-preserved fabrics in SLI are helpful to better understand the early history of deeper-level plutonic complexes in which many textures are erased by prolonged internal movements and crystallization.

2. Structural Subdivisions Scheme

As with many subdivision schemes, the one presented here is fraught with the complexities of mixing description and genesis, together with space and time as they relate to the progressive growth of SLI. We have chosen to first examine structures associated with the openings and modes of magma intrusion-emplacement to build SLI (see overview in Table 1). Our second focus is on structures and fabrics directly related to the growth of the bodies as magma is moving and suspended particles are free to rotate, i.e. the magmatic flow stage (overview in Table 2). Next, we review those fabrics and structures that form after crystals can no longer rotate, but rather respond by solid-state deformation driven by ongoing magmatic processes that are exclusive of external tectonic events (Table 3). Finally, we look at features developing in response to thermal gradients and gravitational forces, as well as marginal structures that help to provide space for magma and that result from fragmentation processes involving igneous and host materials (Table 4).

2.1. Intrusion-related structures

At the onset of opening to build a new SLI, the width of the opening, by definition, starts at nothing and eventually reaches a maximum. Of course subsequent deflation is possible, as is back flow in dykes following loss of driving pressure (Philpotts and Asher 1994). Modes of emplacement involve deformation of the host rocks ranging from purely brittle to purely non-brittle (Schofield et al. 2012b). In the well-lithified portion of the crust, crack propagation is the dominant mechanism by which magma advances, with stresses being concentrated at the crack tip. Steps, bridges and broken bridges (Fig. 1A, B and C) collectively constrain the shapes of intrusions occupying the propagating and transgressing fractures, with offsets in an advancing fracture leading to steps (Rocchi et al. 2007; Schofield et al. 2012b; Thomson and Hutton 2004). Then multiple fractures split off a master fracture in *en echelon* fashion, SLI tend to occur as segments (protolobes) with bridge structures (Fig. 1C) connecting them (Eide et al. 2017; Hutton 2009; Schofield et al. 2012a).

Features occurring at the margins of SLI often reflect geometric patterns associated with the initial emplacement along a developing fracture or fracture system. It is tempting to interpret orientations of forks, branches (apophyses) and anastomosing patterns to constrain flow direction, but such

interpretations cannot generally be used reliably (Rickwood 1990). For example, although the front of an advancing intrusion may bifurcate when a new fracture develops with subparallel orientation, reunion of those fractures along strike would result in not knowing the direction of magma movement.

Dykes can intrude as a single body or as simple sets of dykes, marked by chilled margins on each side. They can also occur as multiple dykes with subsequent intrusion along the same plane producing internal chilled margins of the younger magma. Composite dykes also occur, with distinctly different magmas intruding the same plane more or less synchronously, with or without mixing and mingling effects.

Similarly, subhorizontal sheets can be emplaced as discrete layers, with subsequent sheets above, inside or below previous emplacements (Fig. 1D) (Horsman et al. 2009) (Horsman et al. this volume). Contacts between different sheets can be recognized by the occurrence of lithologic variations, chilling effects, fragmentation or cataclasis (Fig. 1E). In other instances, the time lag between intrusion of successive sheets can be short enough to prevent the oldest intrusion from cooling below its solidus, giving way to a so-called “magmatic contact” that is a diffuse, yet subplanar, surface (Fig. 1F) (Farina et al. 2010; Saint-Blanquat et al. 2006).

For horizontal sills, the classic model for the propagation of magma is by tensile fracturing in the direction of least resistance (Anderson 1938; Gilbert 1877). Based on examples from the Henry Mountains, Utah (USA) it has been proposed that, for viscous magmas, sill thickness is a function of its length, and once a sill reaches a critical aspect ratio of length to overburden thickness it will inflate vertically (Johnson and Pollard 1973; Pollard and Johnson 1973). This vertical inflation stage then leads to the formation of a laccolith. The maximum lateral extent of the initial sill may be controlled by the effective thickness and the elastic properties of the overburden (Jackson and Pollard 1988; Jackson and Pollard 1990; Kerr and Pollard 1998; Koch et al. 1981).

Three models have been proposed for the growth of tabular intrusions such as laccoliths and sills and the expected deformation in the overlying sediments (Corry 1988; Hunt 1953). Model 1 involves a ‘bulldozer’ style of emplacement where the thickness of the intrusion is established early and the magma spreads laterally within a set thickness. This results in extensive disruption of the overlying host rocks, which fold and then unfold as the tip of the advancing magma passes. Model 2 involves simultaneous lateral and vertical growth. This would also result in a deformation history in the roof that records the passage of the magma tip, although it would perhaps be more subdued than in Model 1. Model 3 is the opposite endmember to Model 1 and involves a distinct two-stage process where a thin protosill would propagate to a maximum lateral extent, followed by vertical inflation. This would result in minimal disruption of the roof except close to the tip where the roof will bend, flex and fold, or will fault in a piston-like vertical growth.

A theoretical model applying continuum mechanics has been developed using field observations from the Henry Mountains (Pollard 1973) to explain the formation of peripheral dykes at the tips of laccolith intrusions. In this model, flexural elastic bending of the overburden controlled the intrusion of dykes at the periphery of a laccolith. The depth of formation has been suggested to exert the main control on the development of faults at sill sheet terminations (Thomson and Schofield 2008). In this model, flexural slip folding at shallower depths would favour mechanical failure of the rock through fracture and faulting (Stearns 1978). More recently it has been proposed that a laccolith grown to a certain maximum thickness may subsequently propagate laterally due to its own weight collapsing, resulting in a larger length:thickness ratio (Bunger and Cruden 2011). Other features associated with such a collapse could include decameter-sized graben-horst-like structures on the top surface of a sill (Awdankiewicz et al. 2004).

In other emplacement modes, advance of the magma may be along discrete narrow fractures that develop alongside each other to produce a pattern of fingers (sometimes also called tongues) (Pollard et al. 1975; Stevenson et al. 2007; Thomson and Hutton 2004) that may coalesce and preserve marginal features such as chilling and/or cataclasis (Fig. 1G). Alternatively, a causal, non-brittle relationship between finger formation and fluidisation of country rock has been demonstrated for the Golden Valley Sill in South Africa (Schofield et al. 2010; Schofield et al. 2012b). Structures/shapes similar to cross sections of fingers are beads or apparent boudins that may also develop in dykes and sills as a result of local inflation and/or collapse during or immediately following emplacement in hot country rocks (Fig. 1H) (Bons et al. 2004).

A number of features are seen at a large scale along the margins of sills and laccoliths where the intruding magma defines rounded margins, noted by various authors as tongues (common meaning) and bulbous terminations, sometimes also called lobes (Fig. 1I). These parabolic to semi-circular marginal shapes characterize the lateral and terminal contacts of sheets making up the Maiden Creek, Trachyte Mesa and Black Mesa structures in the Henry Mountains, and are thought to reflect the high surface tension of these viscous magmas in relation to the host material that they were invading (Morgan et al. 2005).

Development of sheets from repeated parallel pulses can produce a series of elongate lobes and provide a good example of the combined distribution of these end member conditions. The flow lobes can be envisaged in the simplest case to be similar to lava flow lobes, where in the core (or along the central axis) there is only constructional flow, and lineations are parallel to the flow direction. Moving away from the core toward the flanks, shearing plays more of a role and planar fabrics become more apparent. At the nose of the lobe only flattening occurs. The disposition of lineations and foliations can be fitted to a series of lobes in this way (Fig. 1J) (Stevenson et al. 2007).

Successive sheet emplacement, leading to subhorizontal SLI such as multi-layered sills and bysmaliths, may involve initial intrusion followed by subsequent intrusion either above or below. Host rock trapped between the resulting layers can generate a sedimentary raft with lateral dimensions in excess of 1 km and thickness >100 m (Schmiedel et al. 2015). Rafts of host material can also develop during dyke formation, and scales of rafts can decrease downward to include screens of wall rock fragments.

Contrasted, but related in scale to large rafts, the arrival of a new magma batch can fail to find a way around or through the initial layer, but can make room by the development of marginal faults along which the body is lifted as a whole (Fig. 1K). For example, the Black Mesa unit in the Henry Mountains is thought to have formed by successive underplating of sheets, with the 1.5 km diameter mass rising on an average of 22 mm/yr by movement on marginal faults (Saint-Blanquat et al. 2006).

Under conditions when tensile fractures migrate explosively by brittle failure in a rigid host material, plumose structures (Fig. 1L) may develop with associated hackle steps and their offsets. These feather-like patterns of ridges and grooves expand outward on the fracture surface in the direction of fracture development, and the tips of the 'feathers' point in the direction of crack propagation (Simón et al. 2006).

A wide variety of localized brittle fracture and faulting systems are associated with intrusive contacts, as would be expected when the crust must make room for new material. Magmas in most SLI arrive with substantial driving pressure, and the units are thickening as more and more magma arrives. These conditions would predictably create transpressive stresses at the contacts, explaining the bends in truncated host foliation, as well as development of Riedel and P fractures (Fig. 1M) (Correa-Gomes et al. 2001). Well-described examples include the Trachyte Mesa intrusion where conjugate sets of high-angle faults with minor offset are cut by *en-echelon* shear fractures (Morgan et al. 2008). More recently, detailed study of deformation bands, faults and tensile joints during three phases of deformation of country rock surrounding the Trachyte Mesa intrusion have constrained a multi-stage model of emplacement(Wilson et al. 2016). Very similar collections of features are preserved on Elba Island in shoreline exposures at the southern edge of a laccolith (Roni et al. 2014) where cataclastic chilled margins and associated breccia are faulted by sprays of low-offset reverse faults.

2.2. Magmatic flow-related structures

Magmatic flow-related structures result from magmatic flow under conditions where particles can rotate freely in response to directed stress, owing to a sufficient amount of melt available in the system (Vernon 2000). Their recognition can be based on orientation and distribution of readily observable

features (i.e. phenocrysts, vesicles, inclusions) or on less tangible characteristics (i.e. AMS, microtextures) (Bouchez 1997; Mock and Jerram 2005; Mock et al. 2003).

2.2.1. Surface structures: Although dykes, sills and laccoliths are, by definition, tabular and sheet-like, detailed examination of their contact surfaces occasionally shows ornamentation such as raised or indented linear features (Fig. 2A; see also Fig. 1L). A number of these parallel linear features are attributed to flow along their alignment (Rickwood 1990; Varga et al. 1998). A group of mesoscopic structures seen most often as flat-topped ridges separated by grooves and termed hot slickenlines are thought to form in the chilled margin as magma moves past irregularities in the wall rock surface with resulting alignment parallel to magma flow (Varga et al. 1998). Earlier workers have described cusps and buds (Pollard et al. 1975), flow lineations (Walker 1987), scour marks (Smith 1987), and fingers (obsolete meaning), grooves and groove molds (Baer and Reches 1987), all thought to form in the direction of flow even if interpretations of formation vary between authors.

An opposing set of linear structures, referred to here as waves and waveforms, also can be found on intrusive surfaces, but aligned at right angles to flow (Fig. 2B). The term 'wave' is here used to describe the shape of these structures, but is in no way implying that they ever actively 'waved' other than during their *in situ* growth as standing stationary waveforms. Previous works have shown that shear forces along the intrusive contact can extend into the host, generating asymmetric drag folds of the contact itself (Fig. 1L) (Correa-Gomes et al. 2001). Reported examples (Rickwood 1990) include: (i) crenulations seen as "microscopic wrinkles to folds a few feet high" on chilled contact surfaces in the Pando porphyry in Colorado (Tweto 1951), and (ii) "flow folds" (Blanchard et al. 1977), "millimetre-high wrinkles projecting out from the glassy surface" (Walker 1987), and asymmetric folds a few millimeters high, sometimes deformed by interfolding of siltstone with igneous rock at Spanish Peaks, Colorado (Smith 1987). These folds have irregular axes but are generally perpendicular to magma flow directions and their asymmetry preserves the sense of flow. Variations in style include roundness and angularity of crests and troughs, disruption along crests so as to form more lobelets (Fig. 2C), and overrunning of crests to produce ropes (Fig. 2D) that have a distinctive pahoehoe-like appearance. These features are discussed below in greater detail in the case study of coherence of structures observed with different methods at different scales. Much smaller features also attributed to drag in the shearing margin of intrusions occur as ropy structures on the lower walls of large, flattened vesicles in basalt of the Whin Sill in northern England (Fig. 2E) (Liss et al. 2002). These have been shown to form with their wave crests perpendicular to flow, and the structures are attributed to shearing of the chilled ductile rind of the vesicles by the underlying magma flow. Similar structures are reported nearby on Holy Island (Liss et al. 2002; Randall and Farmer 1970) and on the Isle of Skye (Schofield et al. this volume).

2.2.2. Internal visibly-oriented features: Included in the flow-related features are those that formed during magma flow when suspended objects (crystals, vesicles, xenoliths, enclaves) were able to rotate in the weaker medium, but while the magma viscosity was sufficient to preserve the alignment (Fernandez and Laporte 1991). Most of these features represent processes and products resulting from filling, transport, and stalling of the magma moving between subparallel walls. Extensive efforts, tracing back at least into the 19th Century (Pirsson 1899), have been made to use fabrics in igneous rocks to deduce their history. Magma flow is the most commonly invoked cause, but it is important to consider other possible origins, including tectonic processes (Paterson et al. 1998), and to carefully separate magmatic flow from non-tectonic solid-state flow (Vernon 2000).

Under conditions of uniform coaxial flow of magma (plug flow), tabular and elongated suspended objects have no motivation to orient themselves preferentially. Therefore, development of a magmatic shape-preferred orientation (SPO) fabric is dependent on conditions of non-uniform flow that produce differential stress acting on such suspended objects, i.e. vesicles or crystals (Fig. 2F, 2G). Non-uniform flow can be thought of with respect to three end members (Fig. 2H): (i) convergent flow as magma moves through a narrowing region and speeds up, (ii) divergent flow as magma spreads laterally with diverging flow lines and slows down, and (iii) non-coaxial flow caused by drag on a boundary surface (Paterson et al. 1998). We can attempt to look at the distribution of these conditions through space and time as a thickening dyke or sheet develops. Initial conditions are dominated by non-coaxial flow with high drag along contacts, but as a sheet thickens by continuing arrival of magma along the interior plane, marginal effects drop off away from the contacts. The stress ellipsoid generated during convergent flow is elongated parallel to the particle path, causing the long axes of suspended phenocrysts to align parallel to these particle paths, while the shortest crystal axes align parallel to the short axis of the ellipsoid. In contrast, crystal orientations resulting from divergent flow tend to be the opposite, with linear fabric forming parallel to stretching and at right angles to the particle paths, while tabular crystals produce planar fabrics representing flattening perpendicular to particle paths. Both of these conditions include stretching and flattening approaching the mode of pure shear.

Some of the easiest fabrics to see in SLI are coming from incorporated foreign material or vesicles that provide distinctive color contrast, rather than from the minerals making up the main rock. These inclusions can be subdivided into two main groups: xenoliths and mafic microgranular enclaves (MME). Xenoliths include solid rock fragments incorporated in the magma, including cognate xenoliths or autoliths, which would include fragments of chilled margin material spalled off into the magma. Interpretation of xenolith and autolith distribution can come not only from their alignment as xenolith screens or trains, but also from their tendency to decrease in size in the direction and sense of magma transport (Fig. 1L) (Correa-Gomes et al. 2001). All these types of xenoliths contrast with MME, which

coexisted as partially molten masses within the host magma and have the potential to change shape in response to stresses in the moving magma. The petrologic characteristics of such materials provide abundant and important information beyond the scope of this work, but their spatial distribution is often compatible with the mineral fabrics described above (Tobisch et al. 1997). Distribution patterns of xenoliths and enclaves can potentially be used to determine the line along which particles/melt were moving, as well as the direction of movement where there is an imbricated arrangement of individual fragments. Interpretation of shapes and orientations of MME must be done with care due to the long-lived and variable histories of these masses (Paterson et al. 2004). Because the rheology of enclaves occurring near each other at the emplacement level often varied dramatically, it is unsafe to assume that their shapes reflect strains associated with development of mineral fabrics. In some cases (Vernon 2000; Vernon et al. 1988), elongation of MME can be demonstrated to correspond to magmatic fabric, with rotation and alignment of plagioclase crystals but without plastic deformation of interstitial quartz. Another caution comes from the recognition that some enclave trains represent a transition from syn-magmatic mafic dykes (Barbarin 2005).

Among the most commonly used mesoscopic-scale structures observable in the field and used as evidence of magma flow are stretched and elongate vesicles (Fig. 2F). These features, presumed to be spherical at the time of inception, deform to define the orientation of the stain ellipsoid in the zone of shear, typically with attitudes corresponding to those revealed by aligned phenocrysts.

Magmatic flow features due to parallel alignment of undeformed phenocrysts and megacrysts, as well as rock fragments (xenoliths) and MME, all in the absence of solid-state matrix strain, may readily be seen at the macroscopic scale. Biotite phenocrysts and microphenocrysts, with their typical oblate shapes, generate a magmatic foliation, while tabular potassium feldspars, and to a lesser degree plagioclase feldspars, generally produce both magmatic foliation and lineation (Fig. 2G). With mafic intrusions, highly elongate minerals such as prismatic amphibole and lath-shaped plagioclase often provide a well-defined magmatic lineation (Fig. 2H). Fabrics near and within xenoliths can help determine a magmatic vs. solid-state origin, since the former produces flow foliation around, rather than through, the xenoliths.

Also associated with the non-coaxial flow regimes along emplacement surfaces are structures related to the process of flowage differentiation (Fig. 2I) by which the percentage of phenocrysts and other suspended objects such as xenoliths and enclaves increases away from the contact (Platten 1995; Ross 1986), generally attributed to the Bagnold effect (Bagnold 1954). Such features are not restricted to dykes, and in fact, are the general rule along the margins of SLI such as the rhyolitic laccolith units of the Halle Volcanic Complex that include thoroughly flow foliated units as well as units with no foliation/alignment (Mock et al. 2003; Schmiedel et al. 2015). These variations are thought to be

controlled by viscosity, with flow foliation developing in the less viscous melts where the density of flow planes is greatest; more highly viscous melts, in contrast, emplace by plug flow with all strain accommodated at the margins of the unit (Breitkreuz et al. this volume).

Near intrusive contacts or in any setting where flow is non-coaxial, general orientations of resulting strain ellipsoids have long axes aligned oblique to the intrusive contact and to the particle flow paths, with the intermediate axes parallel to the wall (Correa-Gomes et al. 2001)). Resulting fabrics include an imbrication (tiling) of tabular crystals and rock fragments (Figs. 1L, 2H), while highly elongate crystals, including those in the groundmass, define a mineral lineation parallel to the direction of maximum stretching. In order to attribute such fabrics to magmatic flow, it is important to confirm that the aligned crystals are internally undeformed (Rickwood 1990; Vernon 2000). Tabular fragments exhibiting mirrored orientations in opposing chilled margins, reflective of their inability to rotate in response to the shear along the margin, can be used to constrain flow direction (Correa-Gomes et al. 2001).

Identifying fabrics in the field can be difficult, especially when the grain size is small or when the fabric is weak. Even when the foliation or planar component is clear, it is nevertheless almost always difficult to constrain the linear component with any degree of certainty. Although phenocryst alignment can be statistically constrained in 2D and then extrapolated to 3D with measurements on orthogonal planes (Bouchez 1997), this process is time-consuming and relies on identifying long axes of phenocrysts by eye.

Techniques involving scanning the internal physical properties of a rock using x-rays and quantifying the shape, distribution and orientation of mineral grains using computed tomography (CT scanning) has been making steady progress over the last decade or so (Cnudde and Boone 2013; Cnudde et al. 2006; Ketcham 2005; Ketcham and Carlson 2001). Also, electron backscatter diffraction techniques have improved efficiency and precision, enabling quantitative fabric analysis in a variety of scenarios and contexts (Prior et al. 2009). However, these techniques remain expensive and restrict data to focused analyses on a few samples.

Another set of flow-related structures, namely magmatic “folds” (Fig. 2J), may form as a true fold following development of one of the fabrics above, or directly as a result of alignment due to differential flow. These features are only rarely recognized in SLI, probably due to their fine-grained nature and apparent homogeneity. A spectacular example of a composite dyke where a combination of flow banding and elongated mafic enclaves defines a parabolic foliation trace indicating horizontal flow within the dyke is reported from Iceland (Eriksson et al. 2011). In a total different lithology, thick sheets of banded aplite preserve internal magmatic folds in the vertical cliffs of Capo Bianco on Elba (Fig. 2J) (Dini et al. 2007). Other examples of magmatic folds come from observations of symmetrical

patterns of imbricated vesicles that merge across the cores of dykes such that the vesicle fabric defines the fold.

2.2.3. Anisotropy of Magnetic Susceptibility: Some structures in igneous bodies cannot be observed or measured directly, and measurement of anisotropy of magnetic susceptibility (AMS) can be of great help in unravelling them. This method, although first highlighted more than 60 years ago (Graham 1954), has remained a somewhat specialist tool despite the advances in measurement precision, accuracy and efficiency (Borradaile and Henry 1997; Martín-Hernández et al. 2004; O'Driscoll et al. 2015; Tarling and Hrouda 1993). The principle behind AMS measurements relies on the physical property of magnetic susceptibility, *K*, which is the relationship between the magnetization, *M,* of a sample in an externally applied magnetic field of strength *H*. It is assumed that in low field strengths, this relationship is linear such that $M = KH$. The anisotropic response is controlled essentially by the SPO and distribution of Fe-bearing phases, principally magnetite and biotite. Magnetite is usually the dominant controlling phase, despite being an accessory phase, because the susceptibility response of this mineral is up to three orders of magnitude stronger than that of biotite.

Although the physics and application of this technique to fabric analysis can be quite nuanced (e.g. presence of inverse fabrics and distinguishing different carriers), numerous studies have shown that the AMS methodology is a very robust and reliable proxy for petrofabric analysis, principally because magnetite tends to form late and interstitially between the main silicate and fabric-forming phases (Archanjo et al. 1995; Grégoire et al. 1998; O'Driscoll et al. 2007; Stevenson et al. 2007).

The anisotropy is controlled by crystallographic features of the mineral phase. Biotite has a platy crystal structure controlled by sheets of silicate tetrahedra, which results in a minimum susceptibility perpendicular to the [001] crystal face. Crystallographic anisotropy of magnetite is less important but is controlled by the octahedral lattice with its axis of preferential magnetism, or "easy" axis, oriented through opposite corners. In magnetite, magnetic behaviour is controlled by grain size and shape. Single-domain and multidomain configurations serve to minimise the external demagnetising field (Fig. 2K.1). Movements of the Bloch wall in multi-domain grains give rise to a magnetisation when an external field is applied (Fig. 2K.2).

The data that is produced from AMS measurement may be visualized as a second order tensor with three orthogonal axes representing the maximum (K1), intermediate (K2) and minimum (K3) susceptibility directions. These eigenvalues can be read as a magnetic fabric where the magnetic foliation is the plane containing K1 and K2 (or normal of K3) and the magnetic lineation is parallel to K1 (Fig. 2L). At the sample scale, all magnetic grains create a magnetic fabric. This is similar to tectonic fabrics and may be interpreted in similar ways. If the fabric is dominantly linear, K2 and K3 are least certain and form a girdle, similar to L tectonite or a Flinn plot k value tending to infinity field (Fig. 2L.1)

(Flinn 1962). When K1>K2>K3, both a foliation and a lineation may be discerned. This fabric is triaxial, similar to a Flinn plot k value close to 1 field (Fig. 2L.2). When K1 and K2 are equally uncertain and form a girdle, K3 is perpendicular to a foliation, similar to an S tectonite or a Flinn plot k value close to 0 field (Fig. 2L.3).

The most useful aspect of AMS analysis is that it can provide excellent and reliable constraint of the linear fabric component. This element is often very difficult to constrain in the field, even when the planar component is very clear. The linear component is nonetheless necessary to determine the maximum stretching direction, which may be fundamental to understanding transport directions (Stevenson and Bennett 2011; Stevenson et al. 2007). The AMS tensor cannot, however, be assumed to have a linear relationship with strain. This relationship is at best semi-quantitative where the shape of the AMS tensor can usually be trusted, but absolute magnitudes are difficult to correlate with strain (Borradaile 1987; Borradaile 1988; Borradaile 1991; Borradaile 2001; Borradaile and Henry 1997; Borradaile and Jackson 2004; Hrouda 1993). This is mainly because the way in which magnetic phases behave and crystallize during and after flow is poorly understood. To help constrain the AMS fabric in relation to the petrofabric, or at least understand what is controlling the AMS so that it can be linked more confidently to the silicate fabric, some form of determination of the magnetic carrier phases is required. This is usually done using temperature versus susceptibility analyses that can identify the presence of magnetite or demonstrate a dominant paramagnetic phase (Liss et al. 2004; Magee et al. 2012; O'Driscoll et al. 2015; Orlický 1990), or by using techniques that are able to separate magnetic anisotropy contributions using low and high field measurements (Richter and van der Pluijm 1994; Stevenson et al. 2007) and various methods using remanence in addition to susceptibility.

Fabric pattern relationships can be summarized with respect to magma flow directions in end on, side view or plan (map) view (Fig. 2M). In each diagram the projected foliation trace is marked with dashed lines and the projected lineation trend with grey lines. Map symbols are shown in plan view to establish fabric geometry in the other diagrams. End on and side views show the plane through which the plan view is taken. In each case there is an upper and lower plane shown respectively in upper and lower parts of the relevant diagram. Grey arrows show the magma flow direction where relevant. Fabric pattern in a magma conduit, like a lava tube (Fig. 2M.1), may represent a lobe, tongue or finger. Foliation trace is generally concentric in end on view but shows a parabolic profile in plan view. Lineation tends to be convergent to a central axis in all views. Fabric patterns for the termination of a sheet in a viscous (non-brittle) propagation mode (Fig. 2M.2) (Schofield et al. 2010; Schofield et al. 2012b). This process may be operating in the country rock associated with fluidisation of the country rocks. Here we assume that sheets take the form of lobes on limited extent along strike, thus in the plan view the lineation trends converge around the nose of the sheet tip. The lobes are flattened in the horizontal plane, so in side view,

projected lineation trends are parallel to the foliation trace, while at tip or nose the lineation are close to perpendicular to the transport direction. If the structure was more cylindrical we may not expect to see lineation along the axis. The fabric patterns expected for a brittle (hydrofracture) propagation mode (Fig. 2M.3) show that there is a zone at the tip of the sheet that is dominated by fluids and we may not see any continuity in the fabric. For a sheet intrusion (Fig. 2M.4), the plumose lineation trend is shown in plan view. Foliation trace displays a parabolic pattern. Here the only places where lineation trends parallel to propagation/magma flow is near the margins and along the central axis. Note that the use of foliation planes, imbricated with respect to the margin (roof or floor), may only be used to determine flow direction along the central axis of flow (much like trough cross bedding in fluvial sandstones).

Two examples of AMS fabric data and their interpretations are reported here for reference. The case of Maiden Creek Sill, Henry Mountains, Utah (Fig. 2N) illustrates lineation trends splaying from an axial trend into a plumose pattern in plan view (Horsman et al. 2005). In contrast, Figure 2O reports AMS data and interpretations from part of the Trawenagh Bay Granite, NW Ireland (Stevenson et al. 2007). Although not for an SLI *per se,* the map highlights the way in which lobes were defined in this intrusion based on foliations curving around a lineation axis. In some lobes the lineation trend was parallel to this axis, in some they tended to splay down flow, and in others the lineation trend seemed to converge down flow.

2.3. Solid-state flow-related structures (syn-magmatic, non-tectonic)

Solid-state flow in magmatic rocks refers to conditions where the igneous system is subjected to stress when it is either fully solidified, or when the amount of melt available is insufficient for crystals to rotate and, therefore, they deform internally (Vernon 2000). We are concerned here with deformation caused by continuing or pulsing emplacement processes rather than from regional tectonic stress. Although this distinction may be difficult to make, examination of fabrics and structures in surrounding host rock is normally sufficient. However, strong differences in rheology, and therefore behavior of the igneous body and its host, can lead to misleading conclusions (Pavlis 1996).

The largest-scale solid-state flow-related features are those that develop along significant expanses of the carapace of SLI as cataclastic shear zones (Fig. 3A) (Habert and Saint Blanquat 2004; Saint-Blanquat et al. 2006), but due to erosion and limited exposure, they normally require effort to characterize. Cataclastic shear can be found more locally on opposing walls of dykes, as well as along the roofs and floors of sills (Schmiedel et al. 2015), or they may form relatively late along flow foliation planes inside emplacing viscous magma (Mock et al. 2003).

These deformation structures are thought to develop within highly viscous chilled margin zones as a result of continued magma flow in the interior of the sheet (Fig. 3B). The thickness of such zones tends

to be measured in centimeters (Horsman et al. 2005; Saint-Blanquat et al. 2006). At the mesoscopic scale, textures could appear as ductile shear (Fig. 3B1, 2, 3), yet at the microscopic scale, crystals are clearly cataclastically deformed, and often show bookshelf textures (Fig. 3B4, 5). Seen on contact surface, these textures are characterised by stretching lineations formed by cataclastically strongly elongated quartz and feldspar crystals (Fig. 3C.1, .2, .3). At Trachyte Mesa, these lineations on the curving terminations of advancing sheets follow the magma surface and are oriented orthogonal to the axes of folds; within a few cm towards the interior, the magmatic foliation abruptly rotates to perpendicular to the contact (Morgan et al. 2008). Similar relations are observed on Elba Island where cataclastically stretched crystals align perpendicular to wave crests (Fig. 3C.2, 3). These lineations in the cataclastic skin of a few cm thickness are also at right angles to those that can occur in the interior, reflecting alignment by non-coaxial shear in the former and by coaxial strain in the latter (Fig. 1F) (Saint-Blanquat et al. 2006). More rarely observed, such zones occur within the interior of SLI where they are attributed to multiple injections of discrete sheets or fingers of younger magma (Horsman et al. 2005; Morgan et al. 2005).

Deformation styles within the cataclastic zones are controlled primarily by mineralogy and gradients of temperature and viscosity. Variation in strain rates can also influence the behavior of minerals. The degree of deformation in the shear zones is at a maximum at the contact and decreases inward. Lineations are the dominant deformation features, owing to the high aspect ratios reached by brittley stretched crystals. A review of sense of motion indicators under magmatic conditions (Blumenfeld and Bouchez 1988) shows that criteria are very similar to those established for solid-state deformation in metamorphic rocks (Simpson and Schmid 1983; Vernon 2004). As implied by referring to these zones as cataclastic, deformation is almost exclusively brittle, but minerals such as biotite can deform plastically as part of a ductile texture (Fig. 3D.1).

Conditions of non-coaxial flow characterize contact zones where magma drags along the host wall and becomes increasingly viscous due to cooling. This creates a simple shear system parallel to the wall and to the particle paths, but with stretching and flattening at an oblique angle. Flow banding can develop in SLI (Fig. 3D.2), for example where the banding defines the plane of overall flow along the margins of bimodal dykes, preserving intercalated mafic and felsic magmas that intruded quasi-contemporaneously (Eriksson et al. 2011).

2.4 Thermal and fragmental structures

Chilled margins are nearly ubiquitous along the contacts of sheet-like bodies emplaced at shallow levels. In fact, initial assumptions about depth of emplacement typically stem from observation of

these marginal features that offer evidence of significant temperature contrast between magma and its host. Confirmation of intrusion, as opposed to extrusion, in some cases comes from observing chilled margins on both walls of these tabular bodies rather than on one. Similarly, chilled margins can be used to unveil post-solidification processes (e.g. faulting) where the margins are truncated. The detailed nature of chilled margins (Fig. 4A), their thickness and degree of crystallinity in particular, is controlled by variables such as magma temperature and composition (and associated viscosity), temperature contrast between magma and host rock, either adjacent to the wall over time or passing along the wall through time. These margins are some of the earliest structures formed during emplacement and often represent the least modified magma.

Another family of features develops in SLI in response to progressive crystallization. These involve mineralogical and textural changes producing layering that parallels the tabular forms. Cooling from the walls of dykes or from the roof and floor of sills and laccoliths often produce changes in matrix grain size, as well as phenocryst size and abundance, particularly in more mafic bodies. Given sufficient thickness and low enough viscosity, crystal settling can generate magmatic layering (Fig. 4B). In the same line, high temperature crystallization domains such as spherulites and lithophysae (Breitkreuz 2013) have been observed to form near the margins of SLI, with the domains often arranged parallel to the margin.

In the case of large mafic SLI, extended duration of crystallization promotes fractionation, with associated development of late magmatic features such as granophyres, pegmatites, and miarolitic cavities (Fig. 4C). Late-stage magmatic products also can form systems of dykes and veins, including development of net-veining. Even in more felsic rocks, such as the rhyolitic laccolith units of the Halle Volcanic Complex, whole rock geochemical zonation can develop due to fluid mobility during groundmass crystallization (Słodczyk et al. 2015).

Contact metamorphic effects associated with SLI emplacement are generally minimal, and a decided lack of contact metamorphic effects is reported as a widespread occurrence (Corry 1988). Based on growth of index minerals, even in thick, high-temperature sheets, effects are decidedly less than for plutonic units of similar size. However, contact effects are particularly important and well documented for mafic sills intruded into organic-rich sediments and sedimentary rocks, with aureole thicknesses generally equal the thickness of the sill (Aarnes et al. 2010). Other studies of contact effects in thinly-bedded laminated carbonate mudstones and organic-rich siltstones report aureoles whose full thickness is recognized only by C and O isotope variations (Dutrow et al. 2001).

At the base of mafic sills intruding wet sediments such as in the Karoo and Newark Basins, spherulitic nodules with bullseye patterns have been observed, with pronounced elemental transfer across bleached zones to the newly stable mineral assemblage in the center. In other settings, heated and

sintered clastic host sediments can develop cooling columns oriented perpendicular to the contact plane (Fig. 4D) (Adamovic 2006). Around most SLI, however, evidence for heated host rock is not visible, perhaps because heat transport away from the SLI contact in porous/permeable host sediments is advective and rapid such that signs of thermal overprint are limited. As an example, vitrinite reflectance from coal seams in the vicinity of large SLI in the Halle Volcanic Complex decreases from values as high as 9 % at the contact to background level within 1.5 m of the contact (Schwab 1962).

Fragmentation structures seen as intrusion contact breccias (Fig. 4E) can develop along the propagating fracture beyond the limits of a sill (Tweto 1951), but more commonly they are found in contact with the intrusive rock (Morgan et al. 2008). These fragmented zones can include the intrusive material, the host material, or both (Schmiedel et al. 2015). Igneous breccia made primarily of intrusive material can develop marginally with fragments cemented by sets or networks of quartz and calcite veins (Awdankiewicz et al. 2004). Breccias at the contact can contain shear bands that conform to the overall direction of magma emplacement (Morgan et al. 2008). These breccias are generated by shear strain at the contact during magma sheet emplacement in response to outward translation of individual sheets, with a large degree of frictional coupling between the overlying layers leading to final brecciation.

Pyroclastic dykes (Fig. 4F) have been described as emplacements in volcanic edifices, as well as in country rock. They may resemble tabular feeding systems of explosive eruptions with the exposure level of the dyke being located above the fragmentation level (Almond 1971; Ekren and Byers 1976). “Ignimbritic dykes” have been documented from high-volume caldera complexes of the Sierra Madre Occidental in Mexico (Aguirre-Díaz and Labarthe-Hernández 2003). Common to these is a vertical orientation of pyroclastic welded domains (fiamme) parallel to the attitude of the dyke, resembling a flow foliation. The typically welded pyroclastic rock forms by lateral aggradation during upwardly directed flow of a dispersion of hot melt fragments and gas. Presumably, these feeding systems are being closed due to deflation of the volcanic complex; otherwise, the lack of porosity in these welded pyroclastic dykes is difficult to comprehend.

Another quite frequent type of clastic dykes are phreatic and phreatomagmatic dykes that are cross-cutting lava flows, pyroclastic deposits or country rock. They display vertically aligned, non-welded domains of fine- to coarse-grained volcanoclastic and non-volcanic fragments (Fig. 4G). These dykes are related to phreatic explosions of water bodies (creeks, lakes, wet substrate) covered by hot lava or pyroclastic flow deposits. Phreatomagmatic dykes may form in the periphery of phreatomagmatic explosions, in and around volcanically active diatremes or emplacing sills and dykes (Martin and Nemeth 2007).

On Elba Island, chaotic breccia zones are preserved with angular fragments of the intruding porphyry and the rigid limestone host material, all 'swimming' in fluidized shale. These types of mixtures can escape the contact zone to form clast-supported breccia dykes (Fig. 4H) in which fragmented intrusive rock mixes with fragmented host rock and intrudes with parallel contacts both into the host and vice versa.

Other pyroclastic systems related to a volcanic vent and formed below the surface may have cone- or pipe-shaped geometry. They range from phreatomagmatic maar-related diatremes to vents related to explosive eruptions of volatile-rich mafic mantle melts (Kano et al. 1997; Reedman et al. 1987). Caution is advised in assuming an intrusive origin when such textures are observed. For example, in the study of a Late Paleozoic silica-rich magmatic system in Burkersdorf, Germany, a detailed 3D data set on orientations of fiamme and cooling columns has been used to justify the interpretation for a welded fall-back breccia in a vent situated on a rhyolitic dyke that propagated subhorizontally through metamorphic country rocks (Winter et al. 2008).

Several variables at the site of emplacement strongly influence the range of disruptive textures that develop in either the intrusive unit or the host, or in both. Foremost among these is the role of fluids, primarily water present in the host, but also as released magmatic fluids. Peperite (Fig. 4I) often forms in adjacent host material when any of a variety of magma types comes in contact with wet sediments, producing a myriad of forms all related as explosive reaction textures that have been well described and illustrated (Martin and Nemeth 2007; Skilling et al. 2002). Pepartitic textures are also reported for interactions of magma and both hydrous salt in the Werra-Fulda Basin, Germany (Schofield et al. 2014) and coal in the Raton Basin, Colorado, USA (Schofield et al. 2012b).

Emplacement of sills and laccoliths into the unconsolidated part of the crust occurs by non-brittle opening of the plane of emplacement, initially dominantly as fingers or lobes with a range of interface fabrics and structures produced (Schofield et al. 2012b). Activation of this emplacement mechanism is apparently restricted to the upper 2 km of the crust and is, in most cases, dependent on induced fluidization by buoyant hot water or vapor producing dispersed grains (Fig. 4J), controlled primarily by fluid volume, host strength, vapor velocity, and clast size (Busby-Spera and White 1987). Fluidization can occur as (i) thermal fluidization, a continuous process with flash boiling of pore-fluids within fluidized material flowing along the magma contact, or (ii) triggered fluidization, when heated pore-fluids are rapidly released by a process not directly related to the magma emplacement, such as a fault, leading to rapid expansion of the pore-fluids (Schofield et al. 2010; Schofield et al. 2012b). These two processes represent end-members and it is likely that in a given intrusion there will be a combination of both processes operating. Such fluidized mixtures of materials can escape to make dykes or pipes that migrate considerable distance into the overlying host (Platten 1984), or if the available fluids and

driving forces are sufficient, to form hydrothermal vent complexes (Fig. 4K) that pierce the overlying strata and sometimes then collapse (Svensen et al. 2006).

As was noted early in this section, chilled margins are characteristic of most SLI, due to the strong temperature contrast with the surrounding host and the generally small volume of many SLI. For similar reasons, formation of post-magmatic, intrusion-scale columnar joints is also common when sheets of solidified magma continue to cool inward from the walls to form parallel prismatic columns. Sets of curved cooling columns can form controlled by non-planar isotherms, parallel to the outer surface of the magma body. Others have examined the detailed fracturing of such jointed rocks in relation to their enhanced porosity in the context of evaluating unconventional hydrocarbon reservoirs (Bermúdez and Delpino 2008).

2.5 Examining Multiple Approaches

Although the above descriptions attempt to simplify the range of conditions and textures, complexity is more likely the norm. Evidence exists for coalescing fingers during dyke and sill formation, and differential rates of flow within a sheet that effectively create magma-magma interface zones in which simple shear and resulting imbrication may occur. Each intrusion needs to be carefully examined to see how the sum of the observations can best be interpreted. As an example, the emplacement history of a giant diabase feeder dyke in Connecticut is reported where seven flow-direction indicators (imbricated phenocrysts, broken and sheared phenocrysts, granophyre wisps emanating from wall rock, granophyre wisps folded by backflow, granophyre segregations attached to phenocrysts, Riedel shears, and ramp structures) have been used to unravel a three-stage model that included back flow (Philpotts and Asher 1994), later confirmed by detailed study of deformed vesicles and AMS analysis (Philpotts and Philpotts 2007).

3. Example of Elba Laccoliths: A Case for Coherence

Many igneous rocks, occurring in dykes and sills in particular, preserve SPO fabrics. However, before concluding that such fabrics are caused by magma flow, other alternatives need to be considered and excluded. If all other reasonable options to generate a fabric are found wanting, then an origin from magma flow becomes most likely. It is worth repeating that the observed fabric mostly represents the flow pattern in the waning stages of movement, and that interpolation to determine earlier patterns during initial emplacement and filling needs to be done with care. On the other hand, given that fabrics

are all related to the flow of magma during the waning stage of emplacement, the data describing their geometries should be coherent, as shown by the example of laccoliths from Elba Island.

3.1. Interior Fabrics and Flow

As with many laccoliths and sills, the laccoliths at Elba Island, Tuscany formed at the transition to horizontal flow following vertical flow in feeder dykes. In such situations, the feeder dykes are characterized by relatively fixed cross sectional area and non-coaxial flow generated by the higher velocity toward the interior, leading to an imbricated fabric. On the other hand, the cross-sectional area of the laccolith bodies continuously increased as the radius and thickness of intrusion increased. Such a transition reoriented the linear and planar fabrics as magma exited the constricting conditions of the dyke and emerged into expanding subhorizontal sheets, a transition similar to that shown experimentally (Kratinová et al. 2006). This observation further underlines that stress fields reconstructed on the basis of mineral fabrics are not sufficient to determine the whole history of flow, because such fabrics represent just the closing stages.

As an example, for the Elba San Martino laccolith, the great coherence between stress fields reconstructed from both (i) orientations of biotite platelets as determined from AMS studies and (ii) aligned tabular K-feldspar megacrysts determined by field analyses (Roni et al. 2014) is nevertheless insufficient to reconstruct the direction and sense of flow. Indeed, the AMS and SPO data provides information about diverging flow lines much like the information provided by simple glacial striations: you know the direction (a line) along which the magma (or ice) moved, but you don't know the sense. Thus, the case of the San Martino laccolith required an initial assumption of overall divergent flow as the laccolith expanded laterally from its feeder dyke, followed by a two-step interpretation. First, the orientation of the flow lines in map view of the laccolith sheets could be determined from the directions of the short axes of the tabular crystals and the weakest AMS direction (K3). Determining the sense of flow along those lines required a second step, namely recognizing that such axes plunged toward or away from flow depending on whether magma was directed toward the base or roof of the laccolith, respectively. The result proved to be a coherent and internally consistent 'geo-logical' pattern, compatible with the original position of the primary feeder dyke (Roni et al. 2014), that is known thanks to the post-emplacement lateral displacement of the laccolith layers that left the feeder dyke and laccolith exposed side by side (Westerman et al. this volume).

3.2 Ornamented Waveforms and Disrupted Contacts

A number of well-exposed intrusive contact surfaces in the Elba laccolith complex provides an opportunity to evaluate the relationship of magma flow to the development of waveforms that are ornamented with cataclastically generated mineral lineations in the outer skin of the porphyries. Observations of these surfaces for both the San Martino and Portoferraio laccoliths show the presence of severely stretched (up to 40:1) phenocrysts of quartz and feldspars (Fig. 3C, 5A). Bookshelf structures in quartz preserve the sense of motion during strain (Fig. 3B5), while feldspar crystals occasionally show similar patterns but are generally characterized by the development of both symmetrical and asymmetrical cataclastic tails of crumbled grains (Roni 2012).

All of these solid-state deformation features, including ductile bending of associated biotite microphenocrysts, are restricted to the outer 1-2 cm of the porphyry (Fig. 5B). The groundmass between the deformed crystals shows no evidence of shearing, appearing only slightly finer grained than the groundmass in the interior of the sheets where the phenocrysts are undeformed. Stretching lineations are commonly present on the upper contacts, but are also seen on basal contacts. Similar structures are reported for shallow intrusions in the Henry Mountains (Horsman et al. 2005; Morgan et al. 2005; Saint-Blanquat et al. 2006).

All examples of these cataclastic lineations on Elba are seen as ornamentation on waveforms that occur along intrusive contact surfaces of porphyry against highly disrupted, or 'fluidized,' shale and serpentinite that has temporarily lost its competence (Fig. 5C). Most commonly, the structures have rounded 'crests' and 'troughs' best described as sinusoidal, but some sets are characterized by pointy crests and/or troughs (Figs. 2B, 3C.3, 5B); elsewhere, crests form with an appearance of having 'overrun' the troughs, producing a small-scale ropy structure with a 'pahoehoe' appearance (Fig. 2D).

Exposures at Elba Island allow also more detailed observation: where host rocks became fluidized, wave sets occur across a range of geometries with wavelengths from 1-2 cm up to 1.5 m, and heights from 0.3 to 33 cm. The largest waveforms are associated with thicker sheets, however smaller waveforms can occur either alone or superimposed to produce sets of waveforms of different orders of magnitude. Relationships of wavelength to amplitude tend to be organized and consistent, displaying a power-law relationship (Fig. 5D).

Additionally, these waveforms on contacts of both the Elba Island and Henry Mountains laccoliths (Horsman et al. 2010), show solid-state phenocryst lineations that are characteristically orientated perpendicular to the axes of the waveforms (Fig. 3C.3, 5A), independent of the regularity of the waveform patterns. And because the lineations wrap on the undulating surfaces, they define the plane perpendicular to those axes. For the Elba laccoliths, the stretching lineation fabric has also been investigated using AMS in the outer 2.5 cm at several contacts, finding that the AMS magnetic lineation (K2) is consistently parallel or sub-parallel to the stretching direction shown by the solid-state fabric on

the contacts (Roni 2012). In addition, both of these lineations, whether measured together or alone, are arranged nearly perpendicular to the axes of associated wave crests. Because the lineation defined by cataclastically stretched crystals is always associated with surface waveforms, and because they invariably occur together, we consider them as directly related to magma flow, with wave crests and troughs aligned perpendicular to flow direction.

Our scenario for the development of these surface features focuses on four elements: fluidization of host rock, sharpness of the contact, freezing the marginal magma, and persisting magma flow. More completely, porphyritic magma enters a brittle fracture, carrying phenocrysts. Host rock is locally fluidized along the fracture but remains "cold" relative to the adjacent, immiscible magma. Magma freezes instantaneously to form a thin skin with embedded phenocrysts. Viscous drag from magma moving against the skin brittley stretches the phenocrysts. The chilled margin thickens incrementally with viscous drag increasing as the sheet also thickens. Crystal stretching extends into the solid and warmer part of the margin, decreasing in intensity. Continued forceful emplacement further thickens the sheet with transpressive forces generating "standing waves" between the warming contact zone and the "soft" host.

With regard to the multiple sets of waveforms, other than having a fluidized host, the main variable most likely controlling both their occurrence and scale is the velocity differential along the flow path, with obstruction of the forward-moving magma causing waveforms to set up behind. In our scenario, lateral propagation was followed by vertical inflation, with two or more episodes during the earliest part of the inflation process. During propagation of the initially thin sheet, the contact surfaces becomes decorated by centimetric waveforms that become preserved in the frozen outer skin of the sheet. Then, subsequent inflation stages did superimpose decimetric- and even metric-scale waveforms on the contacts of the intrusion.

What remains to be fully understood are the fluid mechanics of the coupled system that control the waveform parameter such that wave height and wavelength correlate. Rheological properties of the fluids vary with distance from the contact and with time, and the forms are visualized to have formed as stationary features that never propagated.

3.3. Coherence

If fabrics defined by the preferred orientations of undeformed phenocrysts, by waveforms, and by stretched crystals on contacts are all related to the flow of magma, the data describing their geometries should be internally consistent. These relationships are considered here for a diverging set of particle paths with decelerating magma, such as would occur during growth of a laccolith sheet from a central feeder dyke.

On Elba Island, the observed fabrics present a coherent pattern. First, orientations for tabular K-megacrysts (SPO field measurements) and biotite plates (AMS measurements) within the magmatic sheets are similarly aligned and provide a geologically logical ('geo-logical') pattern of overall magma flow in the interior of sheets (Roni et al. 2014). Second, highly elongated phenocrysts in the skin of the intrusions are stretched parallel to the overall flow lines and are in concordance with AMS lineations measured in cores from exposed contacts. Third, waveforms on intrusive surfaces are aligned perpendicular to those interpreted flow lines, suggesting extension in the direction of flow.

Many of the features described above can offer information about magma flow, but when all of them are available, they provide a coherent geometry of fabrics. For the San Martino laccolith system, expanding sheets of magma were being emplaced under conditions of lateral divergence from a feeder dyke resulting in (i) poles perpendicular to aligned tabular crystals defining the flow direction, (ii) fold axes of wave-like structures aligning perpendicular to flow, and (iii) stretched crystals defining a plane that contains the flow direction which is oriented perpendicular to those fold axes.

4. Concluding summary

Over the past 200 years, a lot of nomenclature has been introduced to describe structures and features of SLIs, often with genetic implications. We have attempted here to organize much of this body of information using logical breaks in the timing of magma emplacement, independent of the scales of features. We started with *Intrusion-related structures* that formed as the magma was initially making space and then developing into its characteristic form. This is followed by a discussion of *Magmatic flow-related structures* that develop as magma moves with suspended crystals that are free to rotate, recognizing that only the final 'snapshot' of this process is preserved. The next set of features were the *Solid-state flow-related structures (syn-magmatic, non-tectonic)* that formed in portions of the intrusions impacted by continuing flow of nearby magma. Our final discussion concerned *Thermal and fragmental structures*, less constrained by time of formation than the other features, but related by their association with creation of space and impact on host materials. While this is not the only scheme possible, we find this reasoned and rational organization to be helpful in describing and interpreting the myriad observations that have been reported.

Acknowledgements

This work has been partially funded by Università di Pisa, grant PRA_2016_33 to SR.

Figure Captions

Figure 1. Intrusion-related structures. (A) Steps – Tridimensional sketch of stepped intrusive layer, either a sill or a dyke; cross sections on the right refers to the lower sketch on the left (Rickwood 1990; Schofield et al. 2012b). (B) Bridges - Sections of wall-rock connecting wall-rock on the two sides of a sill or dyke; cross sections refer to the lower left sketch in Fig. 1A (Hutton 2009; Rickwood 1990; Schofield et al. 2012a). (C) Broken bridges – Stubs of wall-rock remaining after merging of two portions of a dyke or sill (Hutton 2009; Rickwood 1990; Schofield et al. 2012a). (D) Multiple sheeting – An apparently unique intrusion is actually made of two or more intrusive sheets (Leuthold et al. 2013; Leuthold et al. 2012; Michel et al. 2008). (E) Internal contacts - sharp to faint, roughly planar boundaries between similar units of igneous rock, detected by lithologic variations (Leuthold et al. 2013), chilling effects, fragmentation or cataclasis along contacts, or marked by planar arrangement of foreign (host) material (Horsman et al. 2005). (F) Magmatic contact - Diffuse, subplanar surface at the border between two igneous batches, apparently in the interior of an intrusion (Farina et al. 2010; Saint-Blanquat et al. 2006). (G) Fingers – Discrete, flattened cylinders of magma developed alongside each other, eventually coalescing to form a single intrusive layer. (H) Apparent boudins – Beads or apparent boudins in a three-dimensional sketch view of the apparently boudinaged dyke (Bons et al. 2004). (I) Tongues - Bulbous terminations of igneous rock layers, Trachyte Mesa, Henry Mts, Utah (Morgan et al. 2008). (J) Lobes - Elongate **lobes** similar to lava flow units, making up an intrusive unit, Travenagh Bay Granite (Stevenson et al. 2007). (K) Marginal fault – High-angle fault developed at the border of an intrusion, giving way to a bysmalith intrusion shape. (L) Plumose structure - Plume-like fractures flanked by one or two fringe zones of small *en échelon* fractures visible on joint surfaces, and formed during early fracture opening by local stress at fracture tip; useful as an indicator of the direction and sense of fracture propagation. (M) Drag folds, Riedel and P-fractures - Deformation in the host material can be evidenced by deflection/bending/fracturing of the host foliation. Each sketch/picture is after the work indicated by an asterisk in Table 1.

Figure 2. Magmatic flow-related structures. (A) Linear features - mesoscopic linear ornamentations on contacts, parallel to magma flow; slickenlines are reported as an example (Varga et al. 1998). (B) Waves - mesoscopic ornamentations on contacts: elongated, wavy irregularities in the magmatic rock, elongated orthogonal to magma flow; picture from Elba island, Tuscany. (C) Lobelets - mesoscopic ornamentations on contacts: dm-size lobes; picture from Elba island, Tuscany. (D) Ropes - mesoscopic ornamentations on

contacts: pahoehoe-like ropes with dm-size cross-sections; picture from Elba island, Tuscany. (E) Small ropes - mesoscopic ornamentations on contacts: pahoehoe-like ropes with cm-size cross-sections, in a series of nested parabolas, typically found in large vesicles, close to the intrusion outer contact (Liss et al. 2002). (F) Vesicle SPO - parallel to sub-parallel alignment of oblate/prolate vesicles (Liss et al. 2002). (G) Crystal SPO - parallel to sub-parallel alignment (as a foliation or lineation) of undeformed euhedral tabular/prismatic crystals (no solid-state matrix strain; picture from Elba island, Tuscany. (H) Crystal/vesicle SPO – alignment controlled by convergent, divergent and non-coaxial flow (Paterson et al. 1998). (I) Flowage differentiation - variable abundance of phenocrysts, increasing from the border to interior of a tabular intrusion, commonly a dyke. (J) Magmatic folds - bent planes of markers already existing before the end of flow; in this picture, planes defined by dark tourmaline clots in a white aplitic intrusions are bent during the latest stages of flow (Elba Island) (Dini et al. 2007). (K) AMS-magnetisation domains. K.1: Single-domain and multi-domain configurations serving to minimise the external demagnetising field. K.2: Movement of the Bloch wall in multi-domain grains. (L) Magnetic fabric types. L1: Dominantly linear magnetic fabric (similar to an L tectonite). L.2: Both magnetic foliation and lineation discerned. L.3: Magnetic foliation fabric dominant (similar to an S tectonite). (M) Foliation/lineation patterns. M.1: Magnetic fabric pattern of foliations (dashed lines) and lineations (gray lines) in a magma conduit. M.2 and M.3 Fabric patterns proposed for the termination of a sheet in either a viscous or non-brittle propagation mode (Schofield et al. 2010; Schofield et al. 2012b) or a brittle (hydrofracture) propagation mode, respectively. M.4: End on and plan view magnetic foliations and lineations of a sheet intrusion. (N) AMS data and interpretations from the Maiden Creek Sill, Henry Mountains, Utah (Horsman et al. 2005); note plumose splaying of lineation trends. (O) AMS data and interpretations from part of the Trawenagh Bay Granite, NW Ireland (Stevenson et al. 2007); foliation traces are shown in blue and lineation traces in red. Each sketch/picture is after the work indicated by an asterisk in Table 2.

Figure 3. Solid-state flow-related structures (syn-magmatic). (A) Large cataclastic bands/shear zones – schematic drawing of the cataclastic bands in the Black Mesa intrusion, Henry Mts, Utah (Habert and Saint Blanquat 2004). (B) Brittle textures as seen in cross section in the first few cm of the intrusion from the contact. B.1: Top contact of Trachyte Mesa intrusive sheet against sandstone, illustrating a thin, centimetric, shear zone (Morgan et al. 2008). B.2. Top contact of the Portoferraio laccolith, Elba Island, with centimetric shear zone, where quartz and sanidine are cataclastically deformed. B.3: Top contact of Trachyte Mesa intrusive sheet against country rock, illustrating a centimetric shear zone passing to the normal intrusive porphyritic texture with increasing distance from the contact. B.4: Cataclastically deformed plagioclase at the top of the Black Mesa intrusion, Henry Mts (Saint-Blanquat et al. 2006). B5. Book-shelf deformed quartz crystal in the vicinity of contact with country rock of Portoferraio Laccolith,

Elba Island. (C) Brittle textures as seen in plan view on the contact surface. C.1: Solid-state lineation on top of the intrusion, Maiden Creek sill, Henry Mts (Horsman et al. 2005). C.2: Cataclastically stretched feldspar and quartz crystals on the contact surface of the San Martino laccolith, Elba Island. C.3: Cataclastically stretched feldspar and quartz crystals on the contact surface of the Portoferraio laccolith, Elba Island. (D) Ductile textures. D.1: Bent crystal of biotite within a cataclastically deformed portion of an intrusion very close to the contact, with cataclastically stretched feldspar and quartz crystals on the contact surface of the San Martino laccolith, Elba Island (same as Fig. 3B5). D.2: Flow bands – flow banding underlined by trains of mafic enclaves occurring in a more felsic intrusion; arrows (1.) point to the sharp contact between a hybrid zone showing flow banding features in a homogeneous quartz-porphyry; arrows (2.) point to enclaves embedded and flow lineated (Eriksson et al. 2011). Each sketch/picture is after the work indicated by an asterisk in Table 3.

Figure 4. Thermal and fragmental structures. (A) Chilled margins – field photo of a Palaeogene sill with a 5-7 cm chilled margin (slightly finer grained and darker) at the contact against Triassic sandstone, Northern Ireland (notebook is 20 cm long). Mesoscopic picture of a polished slab of the lower contact against pelitic sediments of a Late Paleozoic andesitic sill, with the sill margin vesiculated and bleached, near Magdeburg, Germany (Awdankiewicz et al. 2004). (B) Phenocryst distribution – layering of mafic phases in a felsic level inside a fine-grained gabbro, Gulf of Ajaccio, Corsica. (C) Miarolitic cavities - miarolitic cavity filled with calcite (Cal) and quartz (Qtz) (Saint-Blanquat et al. 2006). (D) Cooling columns - host sediments with cooling columns formed by thermal overprint, close to contact with Late Paleozoic andesitic sill from a quarry west of Magdeburg, Germany. (E) Intrusion contact breccia – white aplite brecciated at the intrusive contact with slightly younger light brown porphyritic laccolith below. Clasts are located in the contact zone, with some migrated tens of cm inside the younger porphyry, coin for scale, Elba Island. (F) Breccia dyke – dyke made of fluidized shale (originally Cretaceous) matrix carrying clasts of late Miocene porphyritic igneous rock and Cretaceous limestone cropping out in the vicinity, coin for scale, Elba Island. (G) Pyroclastic dyke – pyroclastic welded domain with vertically (parallel to dyke attitude) oriented fiamme resembling a flow foliation in a dyke related to the Late Carboniferous Tharandt Forest Caldera, west of Dresden, Germany. (H) Breccia dyke – dyke including fragments of porphyry along with clasts of local and distant host rock, Elba Island, Italy. (I) Peperite – sill with peperite on both sides, Sag Hegy, Hungary. (J) Fluidized material - thermal fluidization (flash boiling within a fluidized mass along the magma contact) and triggered fluidization (rapid release of heated pore-fluids not directly related to magma movement) (Schofield et al. 2012b). (K) Hydrothermal vent complex – full sketch of a vertical section through a hydrothermal vent complex (Svensen et al. 2006) and field photo of the outcropping portion of the Jurassic Witkop hydrothermal vent complex, Karoo. (L) Columnar joints – commonly formed

in SLI when sheets of solidified magma continue to cool inward from the walls to form parallel prismatic columns like mafic sills, example photo from Colca, Peru. Each sketch/picture is after the work indicated by an asterisk in Table 4.

Figure 5. Elba Island laccoliths - (A) Stretching lineations given by extremely deformed crystals on the exposed outer contact surface of the Portoferraio laccolith; coin for scale. (B) Strongly stretched crystals of quartz and feldspars in the outer "skin" (ca. 2 cm) of the Portoferraio laccolith, as seen in cross section on a polished slab. (C) Fluidized black shale amidst lobelets of Portoferraio laccolith in the contact zone; coin for scale. (D) Log-log plot of wavelength and wave height of contact waveform sets, measured at five different locations on Elba Island.

References Cited

Aarnes I, Svensen H, Connolly JAD, Podladchikov YY (2010) How contact metamorphism can trigger global climate changes: Modeling gas generation around igneous sills in sedimentary basins. Geochimica et Cosmochimica Acta 74(24):7179-7195

Adamovic J (2006) Thermal effects of magma emplacement and the origin of columnar jointing in host sandstone. Visual Geoscience:72-74

Aguirre-Díaz GJ, Labarthe-Hernández G (2003) Fissure ignimbrites: Fissure-source origin for voluminous ignimbrites of the Sierra Madre Occidental and its relationship with Basin and Range faulting. Geology 31:773-776

Almond DC (1971) Ignimbrite vents in the Sabaloka cauldron, Sudan. Geol. Mag. 108:159-176

Anderson EM (1938) The dynamics of sheet intrusion. Proceedings of the Royal Society of Edinburgh 58:242-251

Archanjo CJ, Launeau P, Bouchez J-L (1995) Magnetic fabric vs. magnetite and biotite shape fabrics of the magnetite-bearing granite pluton of Gameleiras (Northeast Brazil). Physics of Earth and Planetary Interiors 89:63-75

Awdankiewicz M, Breitkreuz C, Ehling B-C (2004) Emplacement textures in Late Palaeozoic andesite sills of the Flechtingen-Roßlau Block, north of Magdeburg (Germany). In: Breitkreutz C, Petford N (eds) Physical geology of high-level magmatic systems. Geological Society, London, Special Publication, 234, pp 51-66

Baer G, Reches Ze (1987) Flow patterns of magma in dikes, Makhtesh Ramon, Israel. Geology 15(6):569-572

Bagnold RA (1954) Experiments on a gravity-free dispersion of large solid spheres in a Newtonian fluid under shear. Proceedings of the Royal Society of London A225:49-63

Barbarin B (2005) Mafic magmatic enclaves and mafic rocks associated with some granitoids of the central Sierra Nevada batholith, California: nature, origin, and relations with the hosts. Lithos 80(1–4):155-177

Bédard JHJ, Marsh BD, Hersum TG, Naslund HR, Mukasa SB (2007) Large-scale Mechanical Redistribution of Orthopyroxene and Plagioclase in the Basement Sill, Ferrar Dolerites, McMurdo Dry Valleys, Antarctica: Petrological, Mineral-chemical and Field Evidence for Channelized Movement of Crystals and Melt. J. Petrol. 48(12):2289-2326

Bermúdez A, Delpino D (2008) Concentric and radial joint systems within basic sills and their associated porosity enhancement, Neuquén Basin, Argentina. In: Thomson K, Petford N (eds) Structure and Emplacement of High-Level Magmatic Systems. Geological Society, London, Special Publications 302, pp 185-198

Blanchard J-P, Boyer P, GAgny C (1977) Un nouveau critère de sens de mise an place dans une caisse filonienne: le "pincement" des mineraux aux épontes. Tectonophys. 53:1-25

Blumenfeld P, Bouchez J-L (1988) Shear criteria in granite and migmatite deformed in the magmatic and solid states. Journal of Structural Geology 10(4):361-372

Bons PD, Druguet E, Hamann I, Carreras J, Passchier CW (2004) Apparent boudinage in dykes. J. Struct. Geol. 26(4):625-636

Borradaile G (1987) Anisotropy of magnetic susceptibility: rock composition versus strain. Tectonophys. 138:327-329

Borradaile GJ (1988) Magnetic susceptibility, petrofabrics and strain. Tectonophys. 156:1-20

Borradaile GJ (1991) Correlation of strain with anisotropy of magnetic susceptibility (AMS). Pure and Applied Geophysics 135:15-29

Borradaile GJ (2001) Magnetic fabrics and petrofabrics: their orientation distributions and anisotropies. J. Struct. Geol. 23:1581-1596

Borradaile GJ, Henry B (1997) Tectonic applications of magnetic susceptibility and its anisotropy. Earth-Science Reviews 42(1):49-93

Borradaile GJ, Jackson M (2004) Anisotropy of magnetic susceptibility (AMS): magnetic petrofabrics of deformed rocks. In: Martín-Hernández F, Lüneburg CM, Aubourg C, Jackson M (eds) Magnetic fabric: methods and applications. Geological Society, London, Special Publications, 238, pp 299-360

Bouchez J-L (1997) Granite is never isotropic: an introduction to AMS studies of granitic rocks. In: Bouchez J-L, Hutton DHW, Stephens WE (eds) Granites: from segregation of melts to emplacement fabrics. Kluwer, Dordrecht, pp 95-112

Breitkreuz C (2013) Spherulites and lithophysae—200 years of investigation on high-temperature crystallization domains in silica-rich volcanic rocks. Bull. Volc. 75(4):1-16

Breitkreuz C, Petford N (2004) Physical Geology of High-Level Magmatic Systems. In: Geological Society, London, Special Publication, 234, p 253

Bunger AP, Cruden AR (2011) Modeling the growth of laccoliths and large mafic sills: Role of magma body forces. Journal of Geophysical Research 116(B2):B02203

Busby-Spera CJ, White JDL (1987) Variation in peperite textures associated with differing host-sediment properties. Bulletin of Volcanology 49:765-775

Cnudde V, Boone MN (2013) High-resolution X-ray computed tomography in geosciences: A review of the current technology and applications. Earth-Science Reviews 123:1-17

Cnudde V, Masschaele B, Dierick M, Vlassenbroeck J, Van Hoorebeke L, Jacobs P (2006) Recent progress in X-ray CT as a geosciences tool. Applied Geochemistry 21:826-832

Correa-Gomes LC, Souza Filho CR, Martins CJFN, Oliveira EP (2001) Development of symmetrical and asymmetrical fabrics in sheet-like igneous bodies: the role of magma flow and wall-rock displacements in theoretical and natural cases. J. Struct. Geol. 23(9):1415-1428

Corry CE (1988) Laccoliths - Mechanics of emplacement and growth. Geological Society of America Special Paper 220:110

Cruden A, McCaffrey K (2002) Different scaling laws for sills, laccoliths and plutons: mechanical thresholds on roof lifting and floor depression. In: Breitkreuz C, Mock A, Petford N (eds) Physical Geology of Subvolcanic Systems - Laccolith, Sills and Dykes (LASI). Freiberg, 12-14 October 2002, pp 15-17

Cruden AR, McCaffrey KJW (2001) Growth of plutons by floor subsidence: implications for rates of emplacement, intrusion spacing and melt-extraction mechanisms. Phys. Chem. Earth 26:303-315

Dini A, Corretti A, Innocenti F, Rocchi S, Westerman DS (2007) Sooty sweat stains or tourmaline spots? The Argonauts on the Island of Elba (Tuscany) and the spread of Greek trading in the Mediterranean Sea. In: Piccardi L, Masse WB (eds) Myth and Geology. Geological Society, Special Publications, 273, London, pp 227-243

Dutrow BL, Travis BJ, Gable CW, Herny DJ (2001) Coupled heat and silica transport associated with dike intrusion into sedimentary rock: Effects on isotherm location and permeability evolution. Geochimica et Cosmochimica Acta 65:3749-3767

Eide CH, Schofield N, Jerram DA, Howell JA (2017) Basin-scale architecture of deeply emplaced sill complexes: Jameson Land, East Greenland. Journal of the Geological Society 174(1):23-40

Ekren EB, Byers FM (1976) Ash-flow fissure vent in west-central Nevada. Geology 4(4):247-251

Eriksson PI, Riishuus MS, Sigmundsson F, Elming S-k (2011) Magma flow directions inferred from field evidence and magnetic fabric studies of the Streitishvarf composite dike in east Iceland. Journal of Volcanology and Geothermal Research 206(1-2):30-45

Farina F, Dini A, Innocenti F, Rocchi S, Westerman DS (2010) Rapid incremental assembly of the Monte Capanne pluton (Elba Island, Tuscany) by downward stacking of magma sheets. Geological Society of America Bulletin 122(9/10):1463-1479

Fernandez A, Laporte D (1991) Significance of low symmetry fabrics in magmatic rocks. J. Struct. Geol. 13:337-347

Flinn D (1962) On folding during three.dimensional progressive deformation. Quarterly Journal of the Geological Society 118(1-4):385-428

Gilbert GK (1877) Report on the geology of Henry Mountains. In: Department of the Interior, U.S. Geographical and Geological Survey of the Rocky Mountain Region. Washington D.C. Government Printing Office, 160 pp., p 160

Graham JW (1954) Magnetic susceptibility anisotropy, an unexploited petrofabric element. Geol. Soc. Am. Bull. 65:1257-1258

Grégoire V, Darrozes J, Gaillot P, Nédélec A, Launeau P (1998) Magnetite grain shape fabric and distribution anisotropy vs. rock magnetic fabric: A three-dimensional case study, J. Struct. Geol., 20(7), 937–944. J. Struct. Geol. 20:937-944

Habert G, Saint Blanquat Md (2004) Rate of construction of the Black Mesa bysmalith, Henry Mountains, Utah. In: Breitkreutz C, Petford N (eds) Physical Geology of High-Level Magmatic Systems. Geological Society, London, Special Publication 234, pp 163-173

Halls H, Fahrig W (1987) Mafic Dyke Swarms: A Collection of Papers Based on the Proceedings of an International Conference on Mafic Dyke Swarms Held at Erindale College, University of Toronto, Ontario, Canada, June 4 to 7, 1985. Geological Association of Canada.,

Horsman E, Morgan S, Saint Blanquat Md, Tikoff B (2010) Emplacement and Assembly of Shallow Intrusions, Henry Mountains, Southern Utah. In,

Horsman E, Morgan S, Saint-Blanquat Md, Habert G, Hunter R, Nugent A, Tikoff B (2009) Emplacement and assembly of shallow plutons through multiple magma pulses, Henry Mountains, Utah. Earth and Environmental Science Transactions of the Royal Society of Edinburgh 100:1-16

Horsman E, Tikoff B, Morgan S (2005) Emplacement-related fabric and multiple sheets in the Maiden Creek sill, Henry Mountains, Utah, USA. Journal of Structural Geology 27:1426-1444, doi:1410.1016/j.jsg.2005.1403.1003

Hrouda F (1993) Theoretical models of magnetic anisotropy to strain relationship revisited. Phys. Earth Planet. Inter. 77:237-249

Hunt CB (1953) Geology and geography of the Henry Mountains region, Utah. U. S. Geol. Survey Prof. Paper 228

Hutton D (2009) Insights into magmatism in volcanic margins: bridge structures and a new mechanism of basic sill emplacement—

Theron Mountains, Antarctica. Petroleum Geoscience 15:269–278

Jackson MD, Pollard DD (1988) The laccolith-stock controversy: new results from the southern Henry Mountains, Utah. Geological Society of America Bulletin 100:117-139

Jackson MD, Pollard DD (1990) Flexure and faulting of sedimentary host rocks during growth of igneous domes, Henry Mountains, Utah. J. Struct. Geol. 12(2):185-206

Johnson A, Pollard DD (1973) Mechanics of growth of some laccolithic intrusions in the Henry Mountains, Utah, I. Fields observations, Gilbert's model, physical properties and flow of the magma. Tectonophysics 18:261-309

Kano K, Matsuura H, Yamauchi S (1997) Miocene rhyolitic welded tuff infilling a funnel-shaped eruption conduit Shiotani, southeast of Matsue, SW Japan. Bull. Volc. 59(2):125-135

Kerr AD, Pollard DD (1998) Toward more realistic formulations for the analysis of laccoliths. J. Struct. Geol. 20(12):1783-1793

Ketcham RA (2005) Three-dimensional grain fabric measurements using high-resolution X-ray computed tomography. Journal of Structural Geology 27(1217-1228)

Ketcham RA, Carlson WD (2001) Acquisition, optimization and interpretation of X-ray computed tomographic imagery: applications to the geosciences. Computers & Geosciences (27):381-400

Koch FG, Johnson AM, Pollard DD (1981) Monoclinal bending of strata over laccolithic intrusions. Tectonophys. 74(3-4):T21-T31

Kratinová Z, Závada P, Hrouda F, Schulmann K (2006) Non-scaled analogue modelling of AMS development during viscous flow: A simulation on diapir-like structures. Tectonophys. 418(1–2):51-61

Leuthold J, Müntener O, Baumgartner LP, Putlitz B, Chiaradia M (2013) A Detailed Geochemical Study of a Shallow Arc-related Laccolith; the Torres del Paine Mafic Complex (Patagonia). J. Petrol. 54(2):273-303

Leuthold J, Müntener O, Baumgartner LP, Putlitz B, Ovtcharova M, Schaltegger U (2012) Time resolved construction of a bimodal laccolith (Torres del Paine, Patagonia). Earth Planet. Sci. Lett. 325–326(0):85-92

Liss D, Hutton DHW, Owens WH (2002) Ropy flow structures: a neglected indicator of magma-flow direction in sills and dikes. Geology 30(8):715-718

Liss D, Owens WH, Hutton DHW (2004) New palaeomagnetic results from the Whin Sill complex: evidence for a multiple intrusion event and revised virtual geomagnetic poles for the late Carboniferous for the British Isles. J. Geol. Soc., London 161:927-938

Magee C, Stevenson C, O'Driscoll B, Schofield N, McDermott K (2012) An alternative emplacement model for the classic Ardnamurchan cone sheet swarm, NW Scotland, involving lateral magma supply via regional dykes. J. Struct. Geol. 43(0):73-91

Martin U, Nemeth K (2007) Blocky versus fluidal peperite textures developed in volcanic conduits, vents and crater lakes of phreatomagmatic volcanoes in Mio/Pliocene volcanic fields of Western Hungary. J. Volcanol. Geoth. Res. 159(1-3):164-178

Martín-Hernández F, Lüneburg CM, Aubourg C, Jackson M (2004) Magnetic fabric: methods and applications. In: Geological Society, London, Special Publications 238, p 540

McCaffrey KJW, Petford N (1997) Are granitic intrusions scale invariant? J. Geol. Soc., London 154:1-4

Michel J, Baumgartner L, Putlitz B, Schaltegger U, Ovtcharova M (2008) Incremental growth of the Patagonian Torres del Paine laccolith over 90 k.y. Geology 36(6):459-462

Mock A, Jerram DA (2005) Crystal Size Distributions (CSD) in Three Dimensions: Insights from the 3D Reconstruction of a Highly Porphyritic Rhyolite. J. Petrol. 46:1525-1541

Mock A, Jerram DA, Breitkreuz C (2003) Using quantitative textural analysis to understand the emplacement of shallow-level rhyolitic laccoliths – a case study from the Halle Volcanic Complex, Germany. J. Petrol. 44(5):833-849

Morgan S, Horsman E, Tikoff B, Saint Blanquat Md, Habert G (2005) Sheet-like emplacement of satellite laccoliths, sills, and bysmaliths of the Henry Mountains, Southern Utah. In: Field Guide. Geological Society of America, pp 1-28

Morgan S, Stanik A, Horsman E, Tikoff B, de Saint Blanquat M, Habert G (2008) Emplacement of multiple magma sheets and wall rock deformation: Trachyte Mesa intrusion, Henry Mountains, Utah. Journal of Structural Geology 30(4):491-512

O'Driscoll B, Hargraves RB, Emeleus CH, Troll VR, Donaldson CH, Reavy RJ (2007) Magmatic lineations inferred from anisotropy of magnetic susceptibility fabrics in Units 8, 9, and 10 of the Rum Eastern Layered Series, NW Scotland. Lithos 98(1-4):27-44

O'Driscoll B, Ferré EC, Stevenson CT, Magee C (2015) The Significance of Magnetic Fabric in Layered Mafic-Ultramafic Intrusions. In: Charlier B, Namur O, Latypov R, Tegner C (eds) Layered Intrusions. Springer, pp 295-329-

Orlický O (1990) Detection of magnetic carriers in rocks: results of susceptibility changes in powdered rock samples induced by temperature. Detection of magnetic carriers in rocks: results of susceptibility changes in powdered rock samples induced by temperature 63:66-70

Orth K, McPhie J (2003) Textures formed during emplacement and cooling of a Palaeoproterozoic, small-volume rhyolitic sill. J. Volcanol. Geoth. Res. 128:341-362

Paterson SR, Fowler TKJ, Schmidt KL, Yoshinobu AS, Yuan ES, Miller RB (1998) Interpreting magmatic fabric patterns in plutons. Lithos 44:53-82

Paterson SR, Pignotta GS, Vernon RH (2004) The significance of microgranitoid enclave shapes and orientations. J. Struct. Geol. 26(8):1465-1481

Pavlis TL (1996) Fabric development in syn-tectonic intrusive sheets as a consequence of melt-dominated flow and thermal softening of the crust. Tectonophys. 253(1):1-31

Philpotts AR, Asher PM (1994) Magmatic flow-direction indicators in a giant diabase feeder dike, Connecticut. Geology 22(4):363-366

Philpotts AR, Philpotts DE (2007) Upward and downward flow in a camptonite dike as recorded by deformed vesicles and the anisotropy of magnetic susceptibility (AMS). Journal of Volcanology and Geothermal Research 161(1-2):81-94

Pirsson LV (1899) On the phenocrysts of intrusive igneous rocks. American Journal of Science 40:271-280

Platten I (1984) Fluidized mixtures of magma and rock in a late Caledonian breccia dyke and associated breccia pipes in Appin, Scotland. Geol. J. 19:209-226

Platten IM (1995) The significance of phenocryst distributions in chilled margins of dykes and sills for the interpretation of tip processes. In: Baer G, Heimann A (eds) Physics and Chemistry of Dykes. Balkema, Rotterdam, pp 141–150

Pollard DD (1973) Derivation and evaluation of a mechanical model for sheet intrusions. Tectonophysics 19:233-269

Pollard DD, Johnson AM (1973) Mechanics of growth of some laccolithic intrusions in the Henry mountains, Utah, II: Bending and failure of overburden layers and sill formation. Tectonophys. 18(3-4):311-354

Pollard DD, Muller OH, Dockstader DR (1975) The Form and Growth of Fingered Sheet Intrusions. Geol. Soc. Am. Bull. 86(3):351-363

Prior DJ, Mariani E, Wheeler J (2009) EBSD in the earth sciences: applications, common practice, and challenges. In: Schwartz AJ, Kumar M, Adams BL, Field DP (eds) Electron backscatter diffraction in materials science. Springer, pp 345-360

Randall BAO, Farmer N (1970) The Holy Island dyke. Natural History Society of Northumberland Transactions 16:9–91

Reedman AJ, Park KH, Merriman RJ, Kim SE (1987) Welded tuff infilling a volcanic vent at Weolseong, Republic of Korea. Bulletin of Volcanology 49(3):541-546

Richter C, van der Pluijm BA (1994) Separation of paramagnetic and ferrimagnetic susceptibilities using low-temperature magnetic susceptibilities and comparison with high field methods. Phys. Earth Planet. Inter. 82:113-123

Rickwood PC (1990) The anatomy of a dyke and the determination of propagation and magma flow directions. In: Parker AJ, Rickwood PC, Tucker DH (eds) Mafic dykes and emplacement mechanisms. Balkema, Rotterdam

Rocchi S, Dini A, Mazzarini F, Westerman DS (2010) Themed Issue: LASI III–Magma pulses and sheets in tabular intrusions. Geosphere

Rocchi S, Mazzotti A, Marroni M, Pandolfi L, Costantini P, Bertozzi G, di Biase D, Federici F, Lô PG (2007) Detection of Miocene saucer-shaped sills (offshore Senegal) via integrated interpretation of seismic, magnetic and gravity data. Terra Nova 19:232-239

Rocchi S, Westerman DS, Dini A, Farina F (2010) Intrusive sheets and sheeted intrusions at Elba Island (Italy). Geosphere 6(3):225-236

Rocchi S, Westerman DS, Dini A, Innocenti F, Tonarini S (2002) Two-stage laccolith growth at Elba Island (Italy). Geology 30(11):983-986

Roni E (2012) Magma flow in shallow-level laccoliths and their feeder dykes (Elba island and Orciatico, Tuscany) revealed by AMS and structural data. In: PhD thesis, University of Pisa. p 202

Roni E, Westerman DS, Dini A, Stevenson C, Rocchi S (2014) Feeding and growth of a dyke–laccolith system (Elba Island, Italy) from AMS and mineral fabric data. Journal of the Geological Society 171:413-424

Ross ME (1986) Flow differentiation, phenocryst alignment, and compositional trends within a dolerite dike at Rockport, Massachusetts. Geol. Soc. Am. Bull. 97(2):232-240

Saint-Blanquat Md, Habert G, Horsman E, Morgan SS, Tikoff B, Launeau P, Gleizes G (2006) Mechanisms and duration of non-tectonically assisted magma emplacement in the upper crust: The Black Mesa pluton, Henry Mountains, Utah. Tectonophys. 428:1-31

Schmiedel T, Breitkreuz C, Görz I, Ehling BC (2015) Geometry of laccolith margins: 2D and 3D models of the Late Paleozoic Halle Volcanic Complex (Germany). International Journal of Earth Sciences 104(2):323-333

Schofield N, Alsop I, Warren J, Underhill JR, Lehné R, Beer W, Lukas V (2014) Mobilizing salt: Magma-salt interactions. Geology 42(7):599-602

Schofield N, Heaton L, Holford SP, Archer SG, Jackson CA-L, Jolley DW (2012a) Seismic imaging of 'broken bridges': linking seismic to outcrop-scale investigations of intrusive magma lobes. Journal of the Geological Society 169(4):421-426

Schofield N, Stevenson C, Reston T (2010) Magma fingers and host rock fluidization in the emplacement of sills. Geology 38:63-66

Schofield NJ, Brown DJ, Magee C, Stevenson CT (2012b) Sill morphology and comparison of brittle and non-brittle emplacement mechanisms. Journal of the Geological Society 169(2):127-141

Schwab M (1962) Über die Inkohlung der Steinkohlen im nördlichen Saaletrog bei Halle. Geologie 11:917-942

Simón JL, Arlegui LE, Pocoví A (2006) Fringe cracks and plumose structures in layered rocks: stepping senses and their implications for palaeostress interpretation. J. Struct. Geol. 28(6):1103-1113

Simpson C, Schmid SM (1983) An evaluation of criteria to deduce the sense of movement in sheared rocks. Geol. Soc. Am. Bull. 94(11):1281-1288

Skilling IP, White JDL, McPhie J (2002) Peperite: a review of magma-sediment mingling. J. Volcanol. Geoth. Res. 114:1-17

Słodczyk E, Pietranik A, Breitkreuz C, Pędziwiatr A, Bokła M, Schab K, Grodzicka M (2015) Formation of a laccolith by magma pulses: evidence from 1 modal and chemical composition of the 500 m long borehole section through the Permo-Carboniferous Landsberg laccolith (Halle Volcanic Complex). Geochemical Journal 49:523-537

Smith RP (1987) Dyke emplacement at Spanish Peaks, Colorado. In: Halls HC, Fahrig WH (eds) Mafic Dyke Swarms, vol. 34, . Geological Association of Canada Special Paper, pp 47-54

Stearns DW (1978) Faulting and forced folding in the Rocky Mountain foreland. In: Matthews V (ed) Laramide Folding Associated with Basement Block Faulting in the Western United States. Geological Society of America Momoir 151, pp 1-38

Stevenson CTE, Bennett N (2011) The emplacement of the palaeogene mourne granite centres, Northern Ireland: New results from the Western Mourne Centre. J. Geol. Soc., London 168:831-836

Stevenson CTE, Owens WH, Hutton DHW (2007) Flow lobes in granite: The determination of magma flow direction in the Trawenagh Bay Granite, northwestern Ireland, using anisotropy of magnetic susceptibility. Geological Society of America Bulletin 119(11):1368-1386

Stevenson CTE, Owens WH, Hutton DHW, Hood DN, Meighan IG (2007) Laccolithic, as opposed to cauldron subsidence, emplacement of the Eastern Mourne pluton, N. Ireland: evidence from anisotropy of magnetic susceptibility. Journal of the Geological Society 164(1):99-110

Svensen H, Jamtveit B, Planke S, Chevallier L (2006) Structure and evolution of hydrothermal vent complexes in the Karoo Basin, South Africa. J. Geol. Soc., London 163:671-682

Tarling DH, Hrouda F (1993) The Magnetic Anisotropy of Rocks. Chapman & Hall, London,

Thomson K, Hutton D (2004) Geometry and growth of sill complexes: insights using 3D seismic from the North Rockall Trough. Bull. Volc. 66:364-375

Thomson K, Petford N (2008) Structure and Emplacement of High-Level Magmatic Systems. In: Geological Society, London, Special Publication, 302, p 227

Thomson K, Schofield N (2008) Lithological and structural controls on the emplacement and morphology of sills in sedimentary basins. In: Thomson K, Petford N (eds) Structure and Emplacement of High-Level Magmatic Systems. Geological Society, London, Special Publication, 302, pp 31-44

Tobisch OT, McNulty BA, Vernon RH (1997) Microgranitoid enclave swarms in granitic plutons, central Sierra Nevada, California. Lithos 40:321-339

Tweto O (1951) Form and structure of sills near Pando, Colorado. Geological Society of America Bulletin 62(5):507-532

Varga RJ, Gee JS, Staudigel H, Tauxe L (1998) Dike surface lineations as magma flow indicators within the sheeted dike complex of the Troodos Ophiolite, Cyprus. J. Geophys. Res. 103(B3):5241–5256

Vernon RH (2000) Review of Microstructural Evidence of Magmatic and Solid-State Flow. Visual Geosciences 5(2):1-23

Vernon RH (2004) A practical guide to rock microstructure. Cambridge University Press, p 594

Vernon RH, Etheridge MA, Wall VJ (1988) Shape and microstructures of microgranitoid enclaves: indicators of magma mingling and flow. Lithos 22:1-11

Walker G (1987) The dike complex of Koolau volcano, Oahu: internal structure of a Hawaiian rift zone. Volcanism in Hawaii. In: USGS Professional Paper 1350 - Volcanism in Hawaii. pp 961-993

Wilson PI, McCaffrey KJ, Wilson RW, Jarvis I, Holdsworth RE (2016) Deformation structures associated with the Trachyte Mesa intrusion, Henry Mountains, Utah: Implications for sill and laccolith emplacement mechanisms. Journal of Structural Geology 87:30-46

Winter C, Breitkreuz C, Lapp M (2008) Textural analysis of a Late Palaeozoic coherent to pyroclastic rhyolitic dyke system near Burkersdorf (Erzgebirge, Saxony, Germany). In: Thomson K, Petford N (eds) Structure and Emplacement of High-Level Magmatic Systems. Geological Society, London, Special Publication, 302, pp 197-219

Table 1. Emplacement-related structures of shallow-level intrusive bodies - Intrusion-related structures

texture type	description	location	Figure	interpretative notes	examples	References
steps	steps are offsets in propagating and transgressing fractures occupied by magma	leading edge of sills	1a	helps reconstructing the magma propagation direction and sense	Rockall Trough (NE Atlantic)	Rickwood (1990); Hutton (2009); Schofield et al. (2012b)*
bridges	sections of wall-rock connecting wall-rock on the two sides of a sill or dyke	across a dyke or sill	1b	gives info on brittle propagation of magma-filled fractures	Theron Mts (Antarctica)	Schofield et al. (2012b)*; Hutton (2009)
broken bridges	stub of wall-rock projecting from wall-rock into a dyke or sill	in place of a former bridge	1c	gives info on brittle propagation of magma-filled fractures	Theron Mts (Antarctica)	Hutton (2009)*; Schmiedel et al. (2015); Horsman et al. (2005) (at internal contacts)
multiple sheeting	apparently unique intrusion made of two or more intrusive sheets	whole intrusion	1d	evidence for multiple tabular magma pulses in dykes, sills, and laccoliths of any composition	Torres del Paine (Patagonia), Henry Mts (Utah), Elba Isl (Tuscany)	Leuthold et al(2013)*; Horsman et al. (2009); Farina et al (2010); Rocchi et al (2010)
internal contacts	sharp to faint, roughly planar boundary between similar units of igneous rock, sometimes marked by planar arrangement of foreign (host) material	at the border between two igneous batches (apparently in the interior of an intrusion)	1e	evidence for multiple magma pulses in dykes, sills, and laccoliths of any composition	Henry Mts (Utah)	Horsman et al. (2005)*
magmatic contact	diffuse, subplanar surface	at the border between two igneous batches (apparently in the interior of an intrusion)	1f	evidence for short time span between successive intrusions of magma batches	Henry Mts (Utah), Elba Isl (Tuscany)	Saint-Blanquat et al. (2006)*; Farina et al. (2010); this work
fingers	discrete, narrow magma-filled fractures developed alongside each other	lateral contacts between intrusion and host (commonly poorly consolidated sediments)	1g	evidence for multiple magma batches in the form of fingers in mafic/intermediate sills	Golden Valley (Karoo), Raton Basin (Colorado)	Pollard et al. (1975); Schofield et al. (2010), Schofield et al. (2012b)*
boudins (apparent)	beads or boudins as seen in cross-section	dykes or sills	1h	local inflation and/or collapse during or immediately following emplacement in hot country rocks	Cap de Creus (Spain)	Bons et al. (2004)*
tongues	bulbous geometry of the lateral termination of igneous rock layer	sill or laccoliths	1i		Henry Mts (Utah)	Horsman et al (2005); Morgan et al (2008)*
lobes	large elongate lobes, similar to lava flow units	large intrusions	1j	evidence for multiple magma batches in the form of lobes in mafic/intermediate sills	Trawenagh Bay (northern Ireland)	Stevenson et al. (2007)*
marginal faults	high-angle faults	at the border of an intrusion	1k	lifting of the country rock, generating a bysmalith	Henry Mts (Utah)	Saint-Blanquat et al. (2006)*
plumose structures	plume-like fractures flanked by one or two fringe zones of small en échelon fractures	joint surfaces	1l	formed during early fracture opening by local stress at fracture tip; indicates direction and sense of fracture propagation	S Bohemia (Czech Republic)	Simón et al. (2006)*
host foliation drag folds Riedel and P fractures	deflected foliation in the wall rock fractures at high/low angle with the contact	wall rock at the intrusion contact chilled margin of the intrusion	1m	flow direction and sense	Henry Mts (Utah)	Correa-Gomes et al. (2001)*

* in References column indicates the paper the artwork or picture in Figure 1 is from.

Table 2. Emplacement-related structures of shallow-level intrusive bodies - Magmatic flow-related structures

texture type	description	location	Figure	interpretation	examples	References
linear features	mesoscopic elongated ornamentations (irregularities) on contacts: fingers/grooves, groove molds, scour marks, cusp axes, ridges-grooves, hot slickenlines	along intrusion-host rock contact	2a (1l)	found in dykes of basalt to trachyte composition; lineations are parallel to flow direction		Baer and Reches (1987); Varga et al (1998)*
waves	mesoscopic ornamentations on contacts: elongated, wavy irregularities and drag folds in magmatic rock	intrusion's outer skin	2b (1l)	formed early in intermediate to felsic sills and laccoliths; wave axes are orthogonal to flow direction	Elba Isl (Tuscany), Henry Mts (Utah)	Tweto (1951); this work*
lobelets	mesoscopic ornamentations on contacts: dm-size lobes	intrusion's outer skin	2c	formed in felsic sills and laccoliths; interference of disrupting waves	Elba Isl (Tuscany)	this work*
ropes	mesoscopic ornamentations on contacts: pahoehoe-like ropes with dm-size cross-sections	intrusion surface	2d	observed in felsic laccoliths; rope axes orthogonal to flow direction	Elba Isl (Tuscany)	this work*
small ropes	mesoscopic ornamentations on contacts: pahoehoe-like ropes with cm-size cross-sections, in a series of nested parabolas	in large vesicle, close to the intrusion outer contact	2e	formed in mafic sills and dykes by shearing of the ropes by the flow of underlying magma; symmetry axes of ropes parallel to flow direction	Holy Isl - Harkess Rock (NE England)	Randall and Farmer (1970); Liss et al (2002)*
crystal/vesicle SPO (foliation, lineation)	parallel to sub-parallel alignment of undeformed euhedral tabular/prismatic crystals (no solid-state matrix strain) or imbricated oblate/prolate vesicles	(stronger near contacts)	2f 2g 2h			Paterson et al (1989); Paterson et al (1998)*; Vernon (2000); Liss et al (2002)*; Horsman et al (2005); Roni et al (2014)
MME, xenoliths, autholiths trains/ elongation/ alignment	elongate microgranular enclaves (without plastic deformation of the crystals) or small fragments of host rock or autholiths, sometimes organized in trains, sometimes with flow foliation around them		(1l)			Correa-Gomes et al (2001)*
flowage differentiation	Increasing abundance of phenocrysts from the border to interior of a tabular intrusion	most common in the central part of dykes	2i	generated by magmatic flow, that concentrates particles in the zones of highest velocity		Ross (1986)*
magmatic folds	bent planes of markers already existing before the end of flow	anywhere in the intrusion	2j	formed late	Elba Isl (Tuscany), Streitishvarf (Iceland)	Paterson et al (1998); Eriksson JVGR (2011); this work*
crystallographic anysotropy; foliation, lineation	anisotropy of magnetic suscptibility (AMS)		2k			Horsman et al (2005); Roni et al (2014); this work*

* in References culumn indicates the work the sketch/picture in Figure 2 is from.

Table 3. Emplacement-related structures of shallow-level intrusive bodies - Solid-state flow-related structures (syn-magmatic)

texture type	description	location	Figure	interpretation	examples	References
large cataclastic bands	cm- to dm-thick cataclastic shear bands separating thicker layer of undeformed igneous rock	petrographic/physical boundaries (magma host-rock contact or contact between successive magma batches)	3a	boundaries reactivated during successive magma injections	Henry Mts (Utah)	Habert and Saint-Blanquat (2004)*; Saint Blanquat et al (2006)
brittle textures - cross section	stretched /broken/ boudinaged /crushed crystal streaks/ribbons with bookshelf structure; rotation tails; delta-shape crystals; sigma-shape crystals; C-S fabrics; recrystallized "tails"	in the chilled margin at magma host-rock contact or at the contact between successive magma batches	3b		Henry Mts (Utah), Elba Isl (Tuscany)	Habert and Saint-Blanquat (2004); Morgan et al (2005); Horsman et al (2005)*; Saint Blanquat et al (2006); Morgan et al (2008); this work*
brittle textures - plan view		surface contact	3c			
ductile textures	bent crystals, flow bands, streaks	in the chilled margin at magma host-rock contact or at the contact between successive magma batches	3d		Henry Mts (Utah)	Horsman et al (2005); this work*; Eriksson et al. (2011)*

* in References column indicates the work the sketch/picture in Figure 3 is from.

Table 4. Emplacement-related structures of shallow-level intrusive bodies - Thermal and fragmental structures

texture type	description	location	Figure	interpretation	examples	References
chilled margin	fine-grained to glassy intrusion's outermost zone	intrusion border	4a	rapid magma cooling	Scrabo (Northern Ireland), Magdeburg (Germany)	this work*
phenocryst distribution	differential distribution of abundance and/or size of phenocrysts (e.g. magmatic layering, crystal clusters, etc)	intrusion's interior (bottom)	4b	thermal decay, gravity settling	Gulf of Ajaccio (Corsica)	Galerne and Neumann (this Volume)
miarolitic cavities			4c		Henry Mts (Utah)	Saint Blanquat et al (2006)*
cooling columns	columns oriented perpendicular to the contact surface	country rock	4d	effect of heating then cooling of host rock	W Magdeburg (Germany)	this work*
intrusion contact breccia	breccia composed of clast of the host rock(s)	host rock at the bottom or top contact of an intrusive sheet	4e	generated by shear strain at the contact during magma sheet emplacement	Elba Isl (Tuscany)	Morgan et al (2008); Awdankiewicz et al. (2004); this work*
breccia dykes	clast-supported small dykelets	in the intrusion surroundings	4f	phreatic local explosion	Elba Isl (Tuscany)	this work*
pyroclastic dykes	similar to tabular feeding systems of explosive eruptions	volcanic edifices, country rock	4g	welding of pyroclastis occur during upward flow of a dispersion of hot melt fragments and gas	W Dresden (Germany)	Winter et al (2004); this work*
peperite	disintegrated magma mingled with country rock materials	carapace around the intrusion	4h	generated by fragmentation of magma during intrusion in wet sediments, coal and hydrous salt	Sag Hegy (Hungary), Raton Basin (Colorado), Herfa-Neurode (Germany)	Skilling et al. (2002); Awdankiewicz et al. (2004); Schofield et al. (2014); this work*
fluidized material	(i) disaggregated grains (suspended in fluid matrix during fluidization), or (ii) thermally mobalised coal and salt	carapace around the intrusion (fingers), sometimes connected to hydrothermal vents (4j) throughout breccia dykes (4f)	4i	generated by (i) flash boiling of pore fluids during intrusion in wet sediments at depth < ~ 2 km or quick decompression by processes such as faulting, or (ii) thermal mobilization	Whin sill (England), Karoo, Raton Basin (Colorado), Herfa-Neurode (Germany)	Schofield et al (2012b)*; Schofield et al. (2014)
hydrothermal vent complex	clast-supported pipe-like structures up to several hundred metres in diameter, piercing rock layers overlying the intrusion	in the intrusion surroundings, up to significant distance	4j	generated by phreatic explosion following heating of sedimentary pore fluids in thermal aureole around a sill, that leads to fragmentation and collapse and/or upward movement of the overlying rock fragments	Witkop (Karoo)	Jamtveit et al (2004); Svensen et al (2006)*; Svensen et al (this book)
columnar joints	parallel prismatic columns	sills	4k	generated during subsolidus cooling; columns forms orthogonal to the cooling surface; column diameter is inversely proportional to the cooling rate	Colca (Peru), Isle Skye (Scotland)	this work*

A - steps

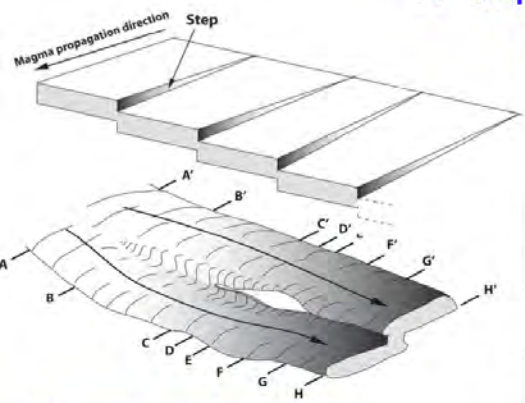

B - bridges

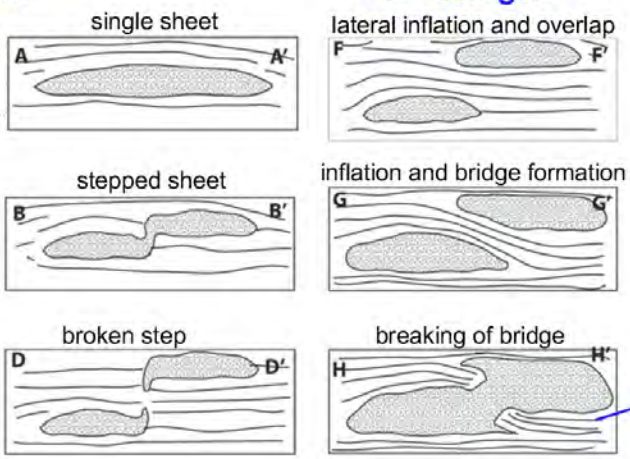

C - broken bridges

D - multiple sheeting

E - internal contacts

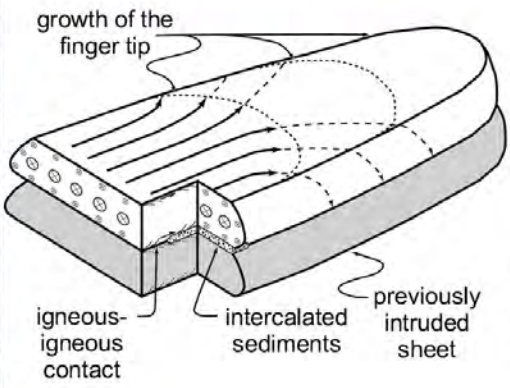

G - fingers

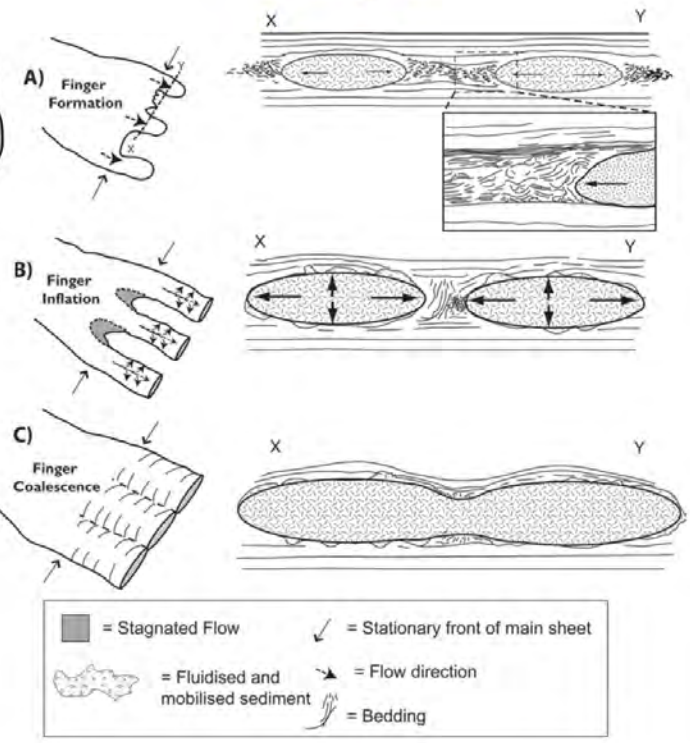

F - magmatic contact

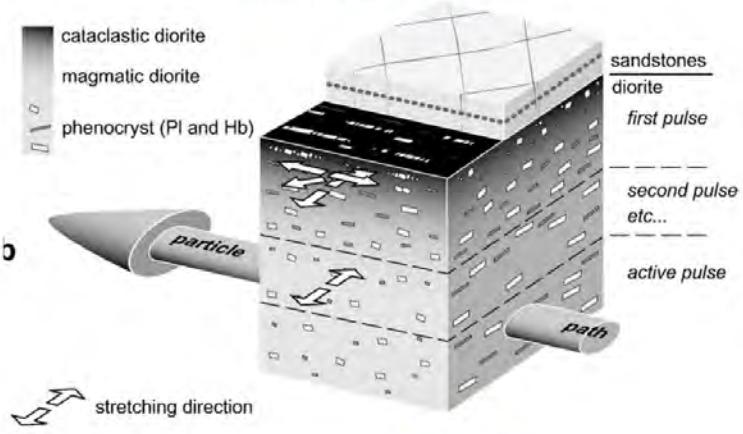

H - apparent boudins

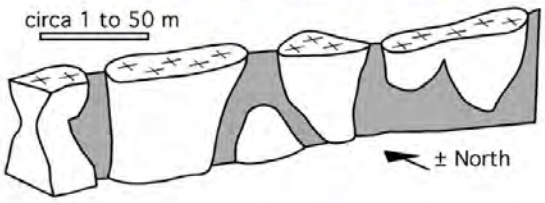

J - lobes

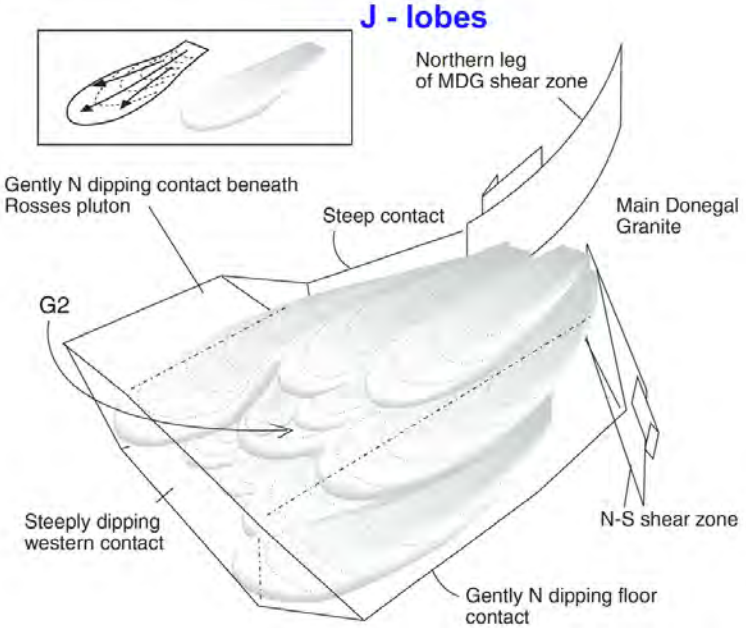

I - tongues

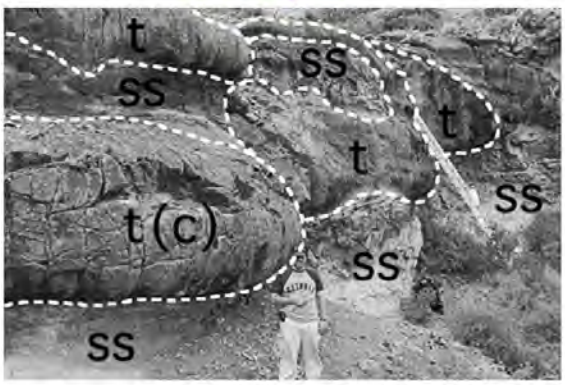

K - marginal fault

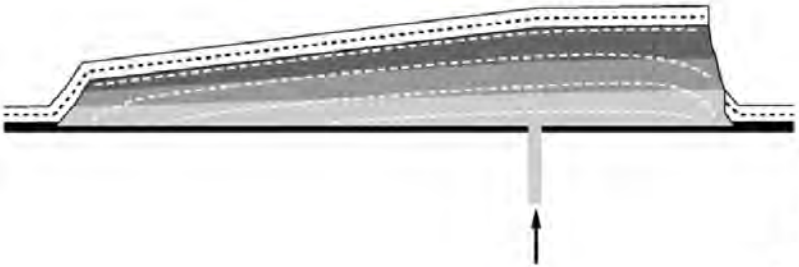

L - plumose structure

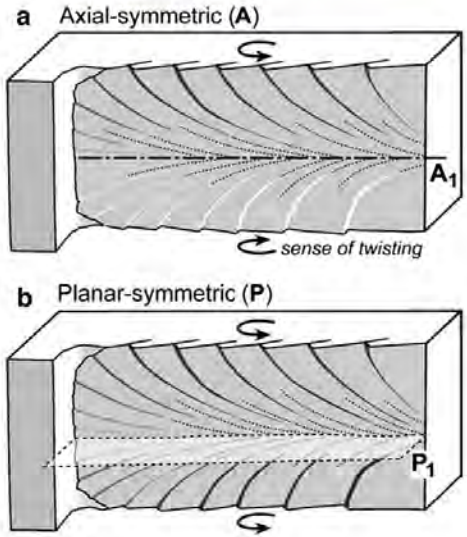

M - drag folds, Riedel and P fractures

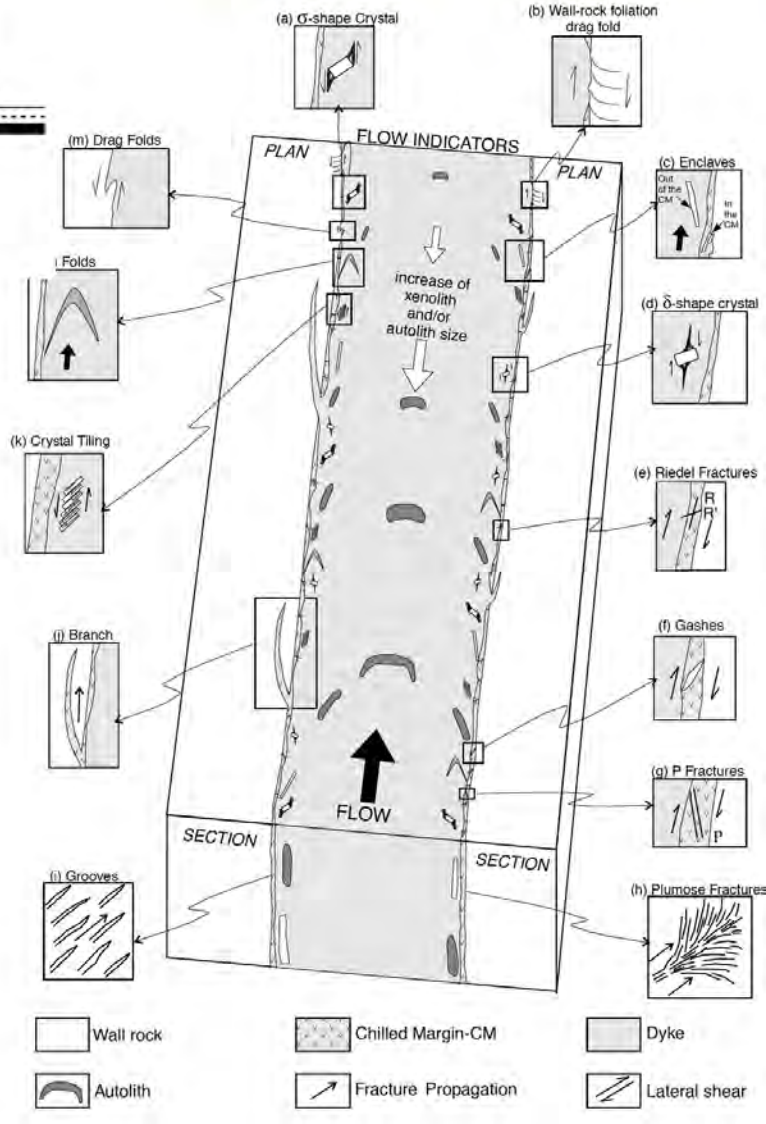

A - linear features

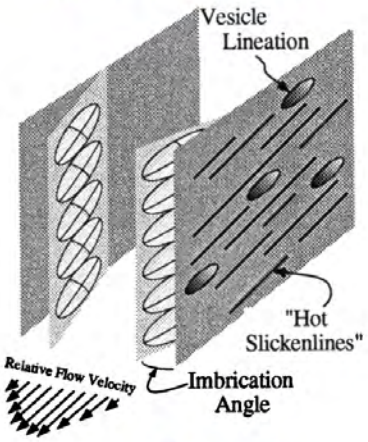

B - waves

C - lobelets

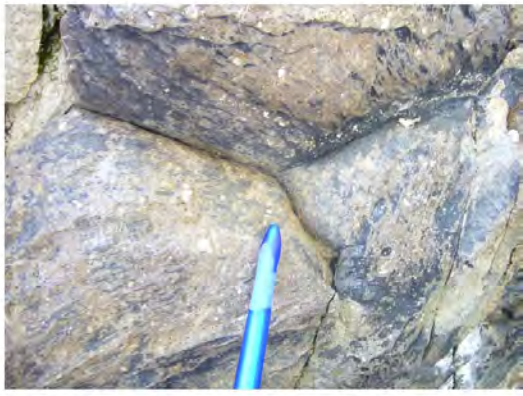

D - ropes

E - small ropes

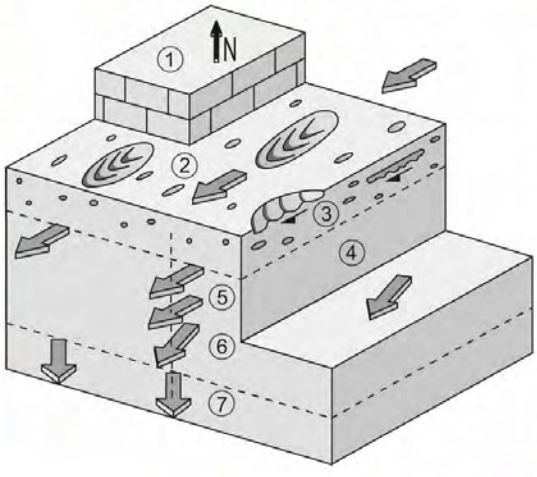

F - vesicle SPO

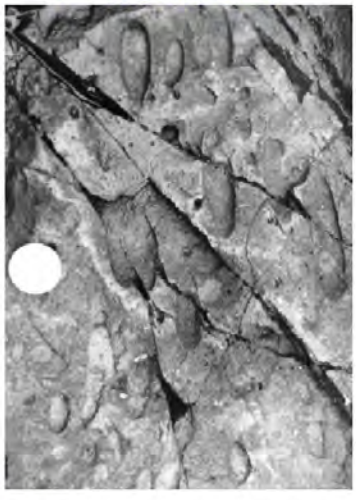

G - crystal SPO

H - crystal/vesicle SPO

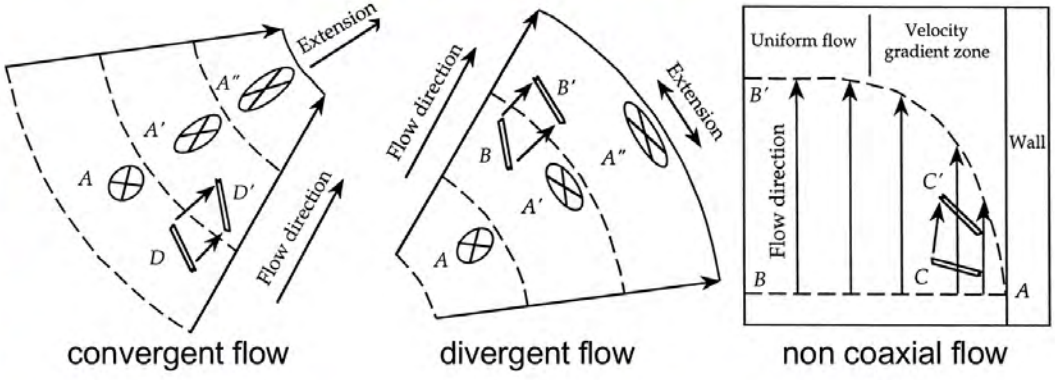

I - flowage differentiation

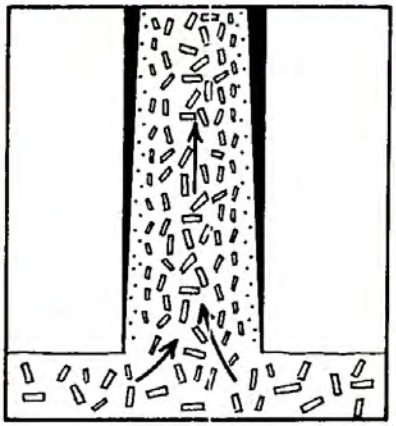

J - magmatic folds

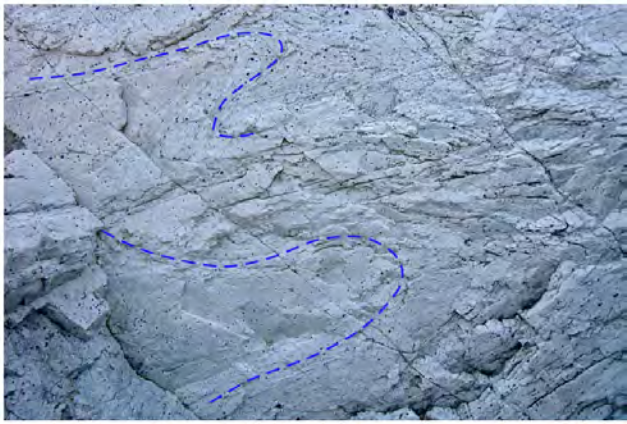

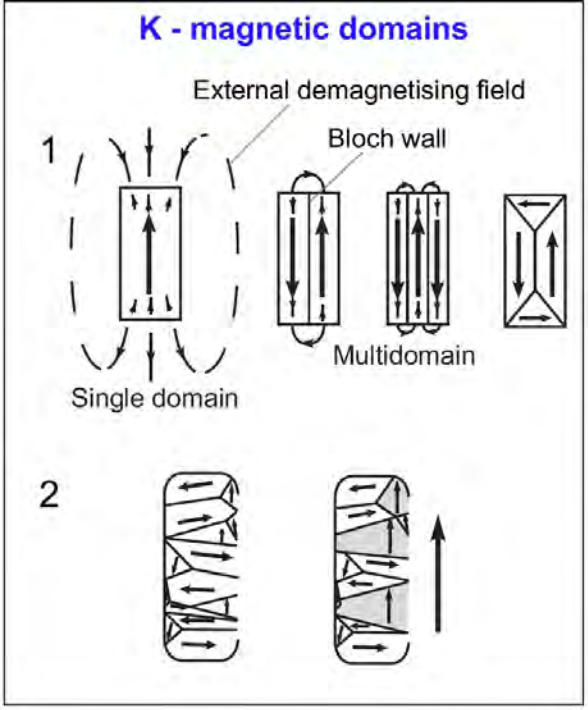
K - magnetic domains
External demagnetising field
Bloch wall
1
Multidomain
Single domain
2

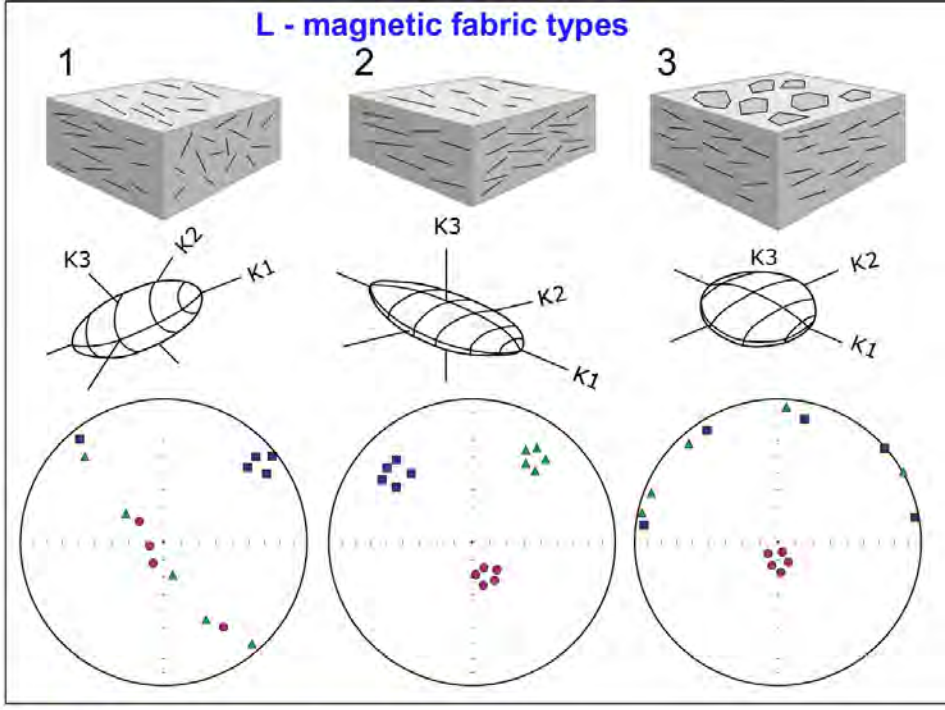
L - magnetic fabric types
1
2
3
K3
K2
K1

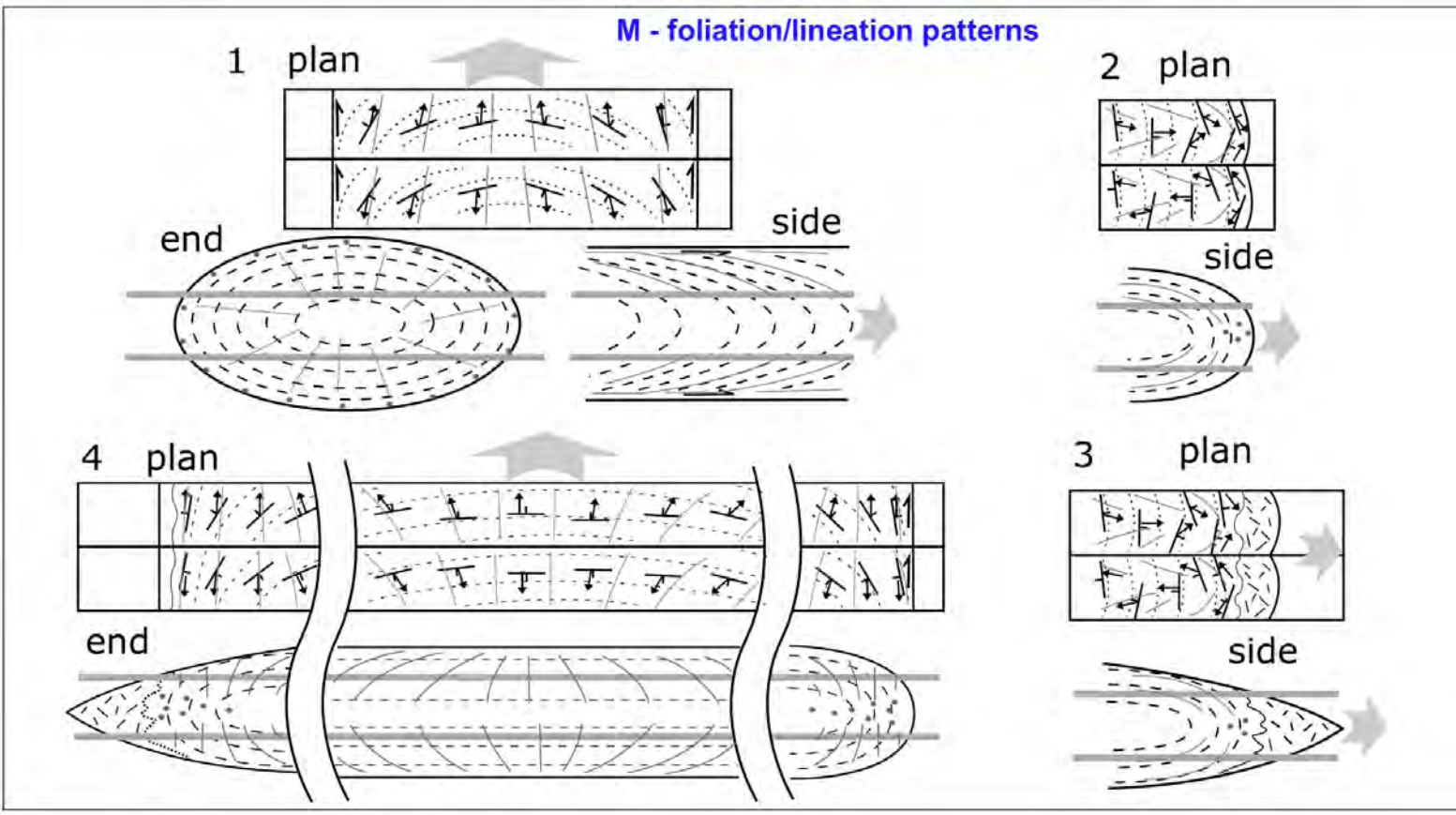
M - foliation/lineation patterns
1 plan
end
side
2 plan
side
4 plan
end
3 plan
side

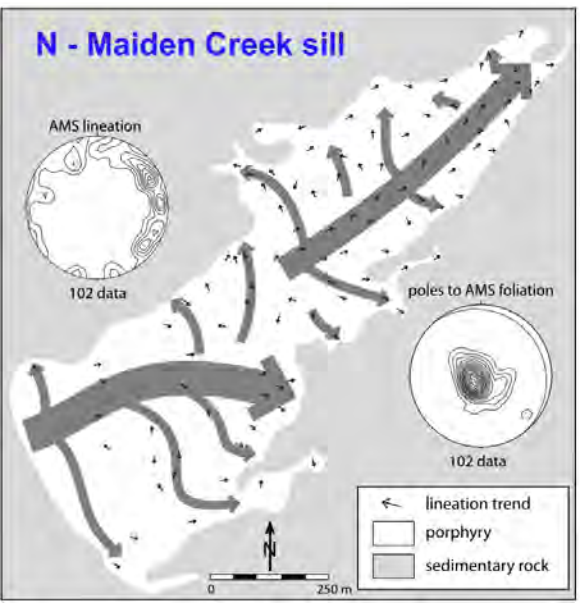
N - Maiden Creek sill
AMS lineation
102 data
poles to AMS foliation
102 data
lineation trend
porphyry
sedimentary rock
N
0
250 m

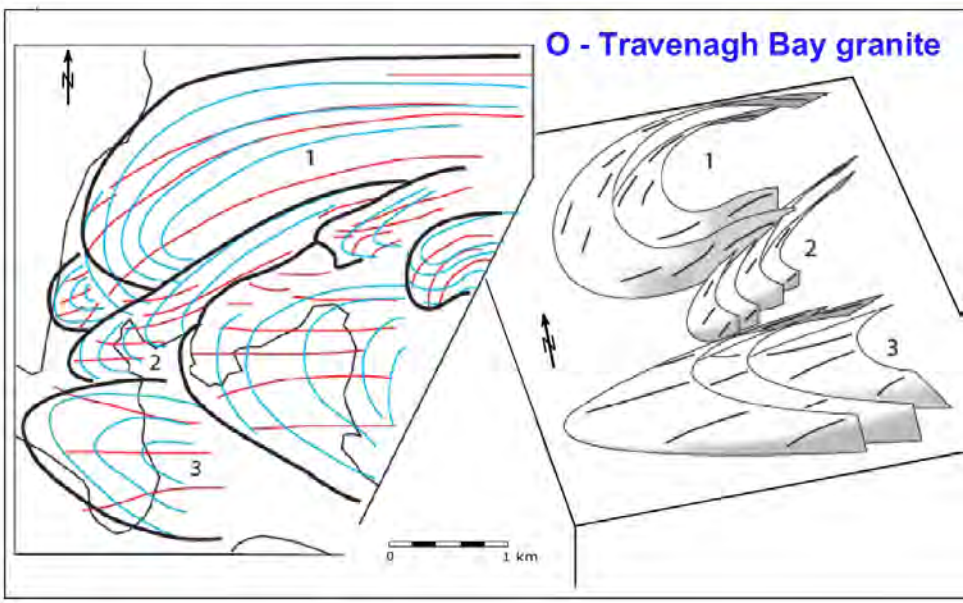
O - Travenagh Bay granite
N
1
2
3
0
1 km

A - cataclastic shear bands

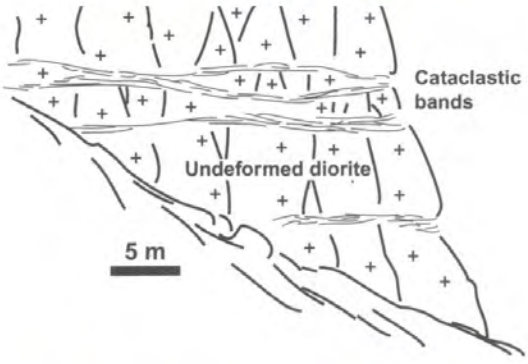

B - brittle textures-cross section

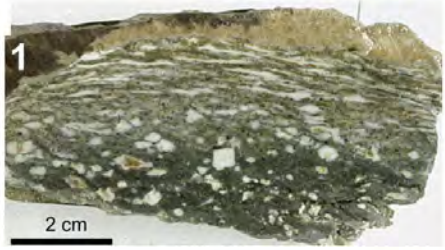

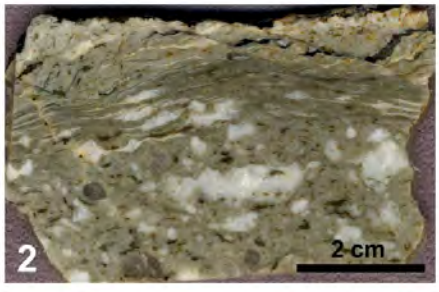

C - brittle textures-plan view

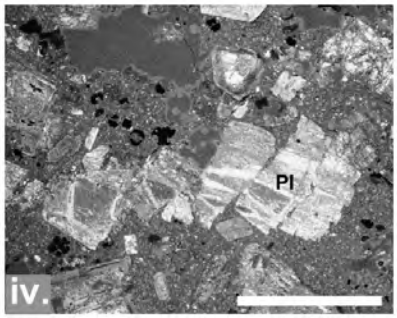

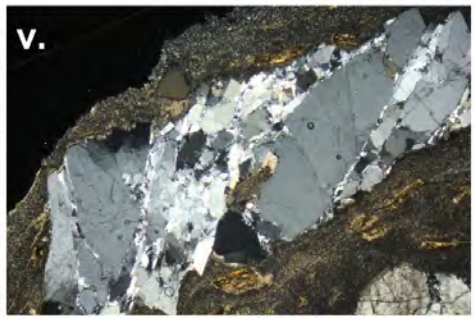

D - ductile textures

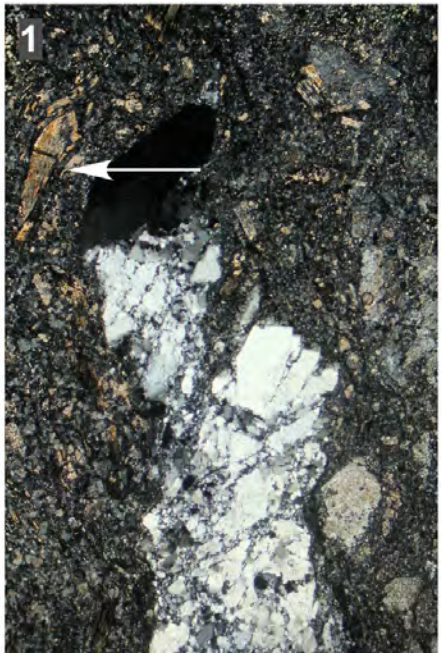

A - chilled margin

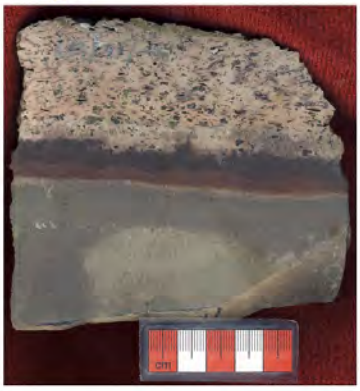

B - phenocryst layering

C - miarolitic cavity

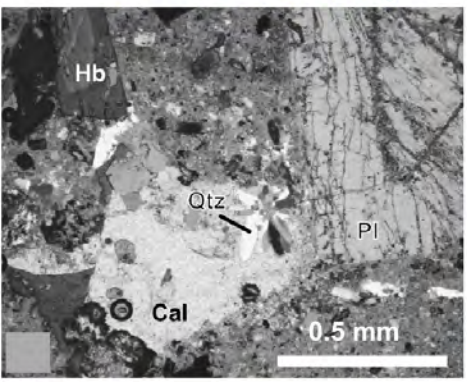

D - cooling columns

E - contact breccia

F - pyroclastic dyke

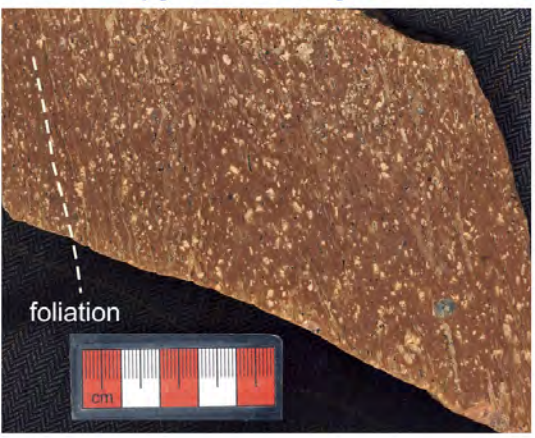

G - phreatomagmatic dyke

H - breccia dyke

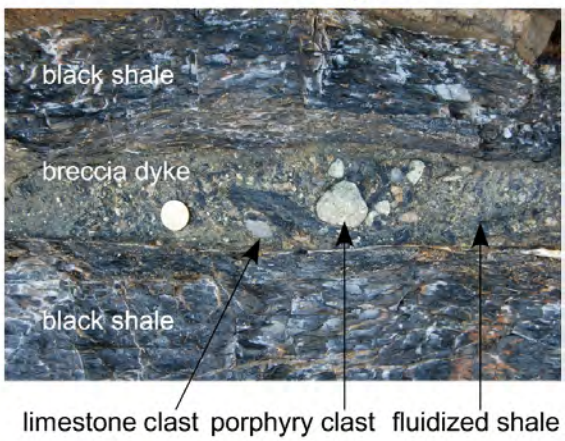

I - peperite

J - fluidized material

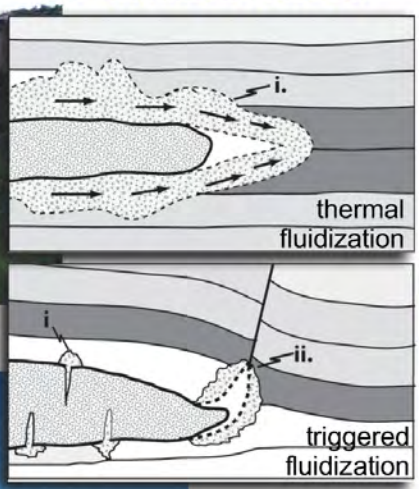

K - hydrothermal vent complex

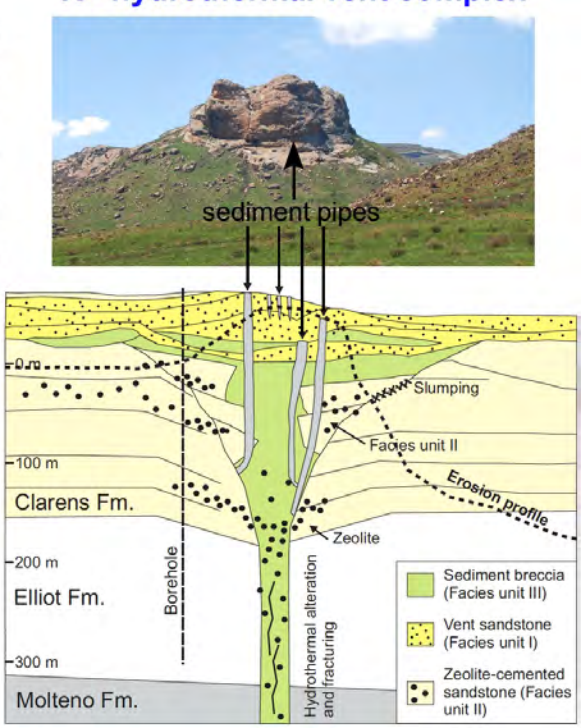

L - columnar joints

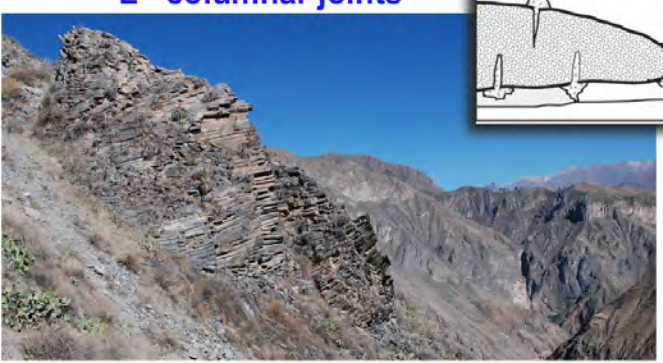


A


B
2 cm


C

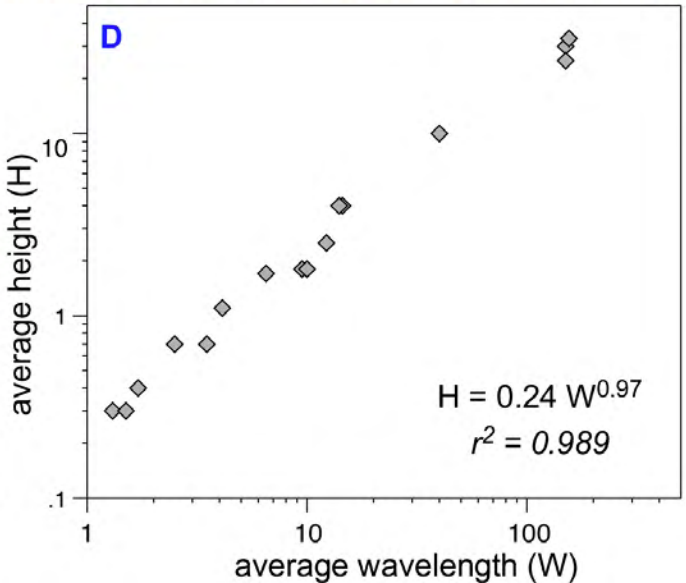
D
average height (H)
10
1
.1
1
10
100
average wavelength (W)
H = 0.24 W0.97
r2 = 0.989